Empirical Features of Spontaneous and Induced Traffic Breakdowns in Free Flow at Highway Bottlenecks

Boris S. Kerner[1], Micha Koller[2], Sergey L. Klenov[3], Hubert Rehborn[2], and Michael Leibel[4]
[1] *Physik von Transport und Verkehr, Universität Duisburg-Essen, 47048 Duisburg, Germany*
[2] *Daimler AG, 71063 Sindelfingen, Germany*
[3] *Moscow Institute of Physics and Technology, Department of Physics, 141700 Dolgoprudny, Moscow Region, Russia and*
[4] *Karlsruhe University of Applied Sciences, 76133 Karlsruhe, Germany*

Based on an empirical study of real field traffic data measured in 1996–2014 through road detectors installed on German freeways, we reveal physical features of empirical nuclei for spontaneous traffic breakdown in free flow at highway bottlenecks. It is shown that the source of a nucleus for traffic breakdown is the solely difference between empirical spontaneous and induced traffic breakdowns at a highway bottleneck. Microscopic traffic simulations with a stochastic traffic flow model in the framework of three-phase theory explain the empirical findings. It turns out that in the most cases, a nucleus for empirical spontaneous traffic breakdown occurs through an interaction of one of waves in free flow with an empirical permanent speed disturbance localized at a highway bottleneck. The wave is a localized structure in free flow, in which the total flow rate is larger and the speed averaged across the highway is smaller than outside the wave. The waves in free flow appear due to oscilations in the percentage of slow vehicles; these waves propagate with the average speed of slow vehicles in free flow (about 85–88 km/h for German highways). Any of the waves exhibits a two-dimensional asymmetric spatiotemporal structure: Wave's characteristics are different in different highway lanes.

PACS numbers: 89.40.-a, 47.54.-r, 64.60.Cn, 05.65.+b

I. INTRODUCTION

In many equilibrium (e.g., [1, 2]) and dissipative metastable systems of natural science (e.g., [3–13]) there can be a spontaneous phase transition from one metastable phase to another metastable phase of a system. Such spontaneous phase transition occurs when a nucleus for the transition appears randomly in an initial metastable phase of the system: The growth of the nucleus leads to the phase transition. The nucleus can be a fluctuation within the initial system phase whose amplitude is equal or larger than an amplitude of a critical nucleus required for spontaneous phase transition. Nuclei for such spontaneous phase transitions can be observed in empirical and experimental studies of many equilibrium and dissipative metastable systems (e.g., [1, 2, 8–13]). There can also be another source for the occurrence of a nucleus, rather than fluctuations: A nucleus can be induced by an external disturbance applied to the initial phase. In this case, the phase transition is called an induced phase transition (e.g., [4, 6, 8–13]).

The occurrence of congestion in vehicular traffic results either from empirical spontaneous or induced traffic breakdown at a highway bottleneck (Fig. 1) [14–16]. An empirical spontaneous traffic breakdown occurs when free flow has been both upstream and downstream before the breakdown has occurred (Fig. 1 (b)). Empirical induced traffic breakdown is caused by a propagation of a localized congested pattern to the bottleneck location; in the case shown in Fig. 1 (c), this localized congested pattern is a moving jam: After the jam is far away upstream of the bottleneck, congested traffic remains at the bottleneck for a long time interval. The downstream front of congested traffic, which separates free flow downstream and congested traffic upstream of the bottleneck, is fixed at the bottleneck. Congested traffic whose downstream front is fixed at the bottleneck is called synchronized flow: Traffic breakdown is a transition from free flow to synchronized flow at the bottleneck (F→S transition) [14, 15].

Because there can be either empirical spontaneous or induced traffic breakdown at the bottleneck (Fig. 1 (b, c)), in three-phase traffic theory is assumed that under conditions $C_{\min} \le q_{\rm sum} < C_{\max}$ free flow is in a metastable state with respect to an F→S transition at the bottleneck, where $q_{\rm sum}$ is the flow rate in free flow at the bottleneck, $C_{\min}$ and $C_{\max}$ are, respectively, some minimum capacity and maximum capacity of free flow at the bottleneck [14–16]. This means that in an empirical example shown in Fig. 1 (d), in which due to jam propagation through the bottleneck *no* traffic breakdown has been induced at the bottleneck, condition $q_{\rm sum} < C_{\min}$ should be satisfied.

As in other metastable systems, we could expect that when an empirical spontaneous traffic breakdown is observed, there should also be a disturbance in free flow that acts as a nucleus for the F→S transition (traffic breakdown) at the bottleneck. However, up to now no nuclei, which are responsible for spontaneous traffic breakdown at highway bottlenecks, could be identified in real field traffic data measured in free flow. In this article, we reveal empirical nuclei for spontaneous traffic breakdown in free flow at highway bottlenecks and study their physics.

The article is organized as follows. The physics of empirical nuclei for spontaneous traffic breakdown at highway bottlenecks is the subject of Sec. II. An empirical

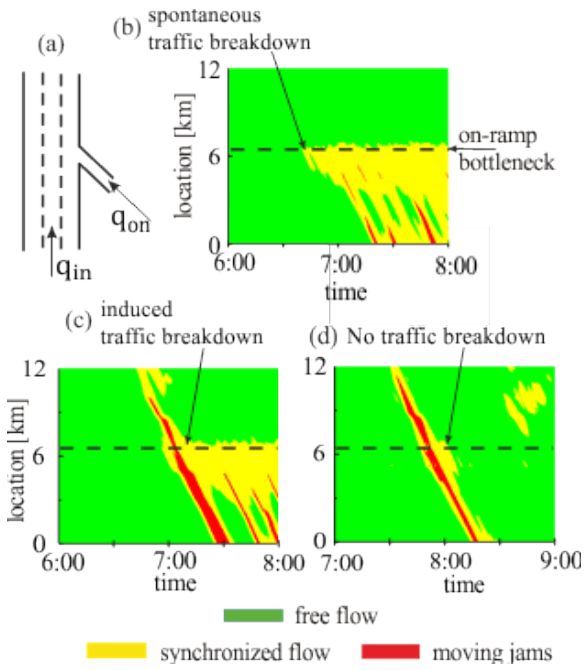

FIG. 1: Overview of empirical features of traffic breakdown (F→S transition) at an on-ramp bottleneck: (a) Sketch of section of three-lane highway in Germany with an on-ramp bottleneck. (b–d) Speed data measured with road detectors installed along road section in (a); data is presented in space and time with averaging method described in Sec. C.2 of [17]. (b) Empirical spontaneous traffic breakdown. (c) Empirical induced traffic breakdown. (d) Moving jam propagation through the bottleneck without induced traffic breakdown. Real field traffic data measured by road detectors on three-lane freeway A5-South in Germany on April 15, 1996 (b), March 22, 2001 (c), and June 23, 1998 (d). On-ramp bottleneck marked by dashed lines in (b–d) is effective on-ramp bottleneck B_3 explained in detailed in Sec. 9.2.1 of [14]. Road detectors, at which 1-min traffic data averaged across the road presented in (b–d) have been measured, are at locations: $x =$ 0, 1.7, 3.2, 4.7, 5.1, 6.4, 7.9, 8.8, 9.8, 11.1, 12.2 km.

spatiotemporal structure of nuclei and a microscopic theory of the nucleation of traffic breakdown at highway bottlenecks are considered in Sec. III. In Sec. IV, we discuss empirical features of different sources of nuclei for empirical traffic breakdown at highway bottlenecks (Secs. IV A and IV B) as well as formulate conclusions.

II. PHYSICS OF EMPIRICAL NUCLEATION OF TRAFFIC BREAKDOWN AT HIGHWAY BOTTLENECKS

A. Methodology of study of waves in empirical free flow

In each of the freeway lanes, road detectors measure the following 1-min averaged data: the flow rate of all vehicles q, the flow rate of long vehicles $q_{\rm slow}$, and the average speed v; respectively, we can calculate the percentage of long vehicles $\psi = 100 q_{\rm slow}/q$ that can be considered *slow vehicles* because the most of long vehicles moving on working days on German highways have a speed limit 80 km/h (in reality, slow vehicles move usually at the speed within a range 80–90 km/h).

To find nuclei for traffic breakdown, we study possible waves in free flow. Additionally with possible waves of 1-min average traffic variables q, $q_{\rm slow}$, v, and ψ, we inverstigate also waves of the following variables

$$\Delta q_{\rm wave} = q - \bar{q},\ \Delta\psi_{\rm wave} = \psi - \bar{\psi},\ \text{and}\ \ \Delta v_{\rm wave} = \bar{v} - v, \tag{1}$$

where traffic variables $\bar{q}$, $\bar{v}$, $\bar{\psi}$ are related to 20-min average data with the used of the well-known procedure of "moving averaging".

Furthermore, to reconstruct a possible wave propagation in space and time, we consider a pair of road detectors whose co-ordinates are $x = x_{\rm up}$ (upstream detector) and $x_{\rm down}$ (downstream). We denote traffic variables measured by these detectors by $\varphi(x_{\rm up},\ t)$ and $\varphi(x_{\rm down},\ t)$ for the upstream and downstream detectors, respectively, i.e., φ denotes one of traffic variables:

$$\varphi = [\Delta q_{\rm wave},\ \Delta v_{\rm wave},\ \Delta\psi_{\rm wave},\ q,\ q_{\rm slow},\ v,\ \psi]. \tag{2}$$

Within road locations x between these two detectors

$$x_{\rm up} < x < x_{\rm down}, \tag{3}$$

we introduce K *virtual* road locations ($K \gg 1$) with coordinates x_i that are at a small distance Δd each from another, where $i = 1, 2, ..., K$, $\Delta d = (x_{\rm down} - x_{\rm up})/K$. Then traffic variables φ (2) at each of locations x_i are found from formula:

$$\varphi(x_i, t) = \frac{x_{\rm down} - x_i}{x_{\rm down} - x_{\rm up}} \varphi(x_{\rm up},\ t + \frac{x_{\rm up} - x_i}{v_{\rm d}}) + \frac{x_i - x_{\rm up}}{x_{\rm down} - x_{\rm up}} \varphi(x_{\rm down},\ t + \frac{x_{\rm down} - x_i}{v_{\rm d}}), \tag{4}$$

where $v_{\rm d}$ is constant model parameter. Some results of such analysis of empirical waves in free flow are presented in Figs. 2 and 3. We have found that empirical waves can propagate through the whole road section; some of the waves appear at on-ramps or disappear at off-ramps.

In Fig. 2, we observe a strong increase in the flow rates q and $q_{\rm Lslow}$ in the flow direction that begins about 0.5–1 km upstream of the effective location of the on-ramp bottleneck labeled by "on-ramp bottleneck" in Fig. 1 (b) [18]. Due to this increase in the flow rate, the average speed decreases appreciably.

To avoid this negative impact of average values of traffic variables on wave resolution in free flow (Fig. 2), in Fig. 3 we present waves of variables $\Delta\psi_{\rm wave}$, $\Delta q_{\rm wave}$, and $\Delta v_{\rm wave}$ (1). Then we find out that the waves of the flow rate $\Delta q_{\rm wave}$ and the speed $\Delta v_{\rm wave}$ almost coincide with the waves of the percentage of (slow) long vehicles $\Delta\psi_{\rm wave}$ (Fig. 3).

We see that each of the waves of the traffic variables (2) propagates downstream with the mean wave velocity $v_{\rm wave}$ that is approximately equal to the mean speed of slow vehicles $v_{\rm slow}^{\rm (mean)}$ (Figs. 2 and 3):

$$v_{\rm wave} = v_{\rm slow}^{\rm (mean)}. \qquad (5)$$

In all empirical data, $v_{\rm slow}^{\rm (mean)}$ is given by the average speed of long vehicles that changes within range 85–88 km/h. Within any of the waves propagating with the velocity $v_{\rm wave}$ (5) the percentage of long vehicles and the flow rate are larger, whereas the average speed is lower than outside the wave.

B. Empirical nucleation of traffic breakdown at on-ramp bottleneck

During a long time interval, the waves of traffic variables in free flow propagate with the positive velocity $v_{\rm wave}$ (5) through the on-ramp bottleneck without any consequences for free flow at the bottleneck (Fig. 3). This changes crucially when we consider a longer time interval (Fig. 4).

Indeed, when one of the waves propagates through the on-ramp bottleneck, the wave initiates traffic breakdown at the bottleneck. During the subsequent wave propagation downstream of the bottleneck, the structure of the wave and its features do not change. Thus, one of the waves in free flow studied above becomes to be a nucleus for traffic breakdown at the bottleneck, when the wave propagates through the bottleneck (labeled by "nucleus" in Fig. 4 (c)).

C. Empirical nucleation of traffic breakdown at off-ramp bottleneck

The empirical result shown in Fig. 4 remains qualitatively the same for the case of wave propagation through

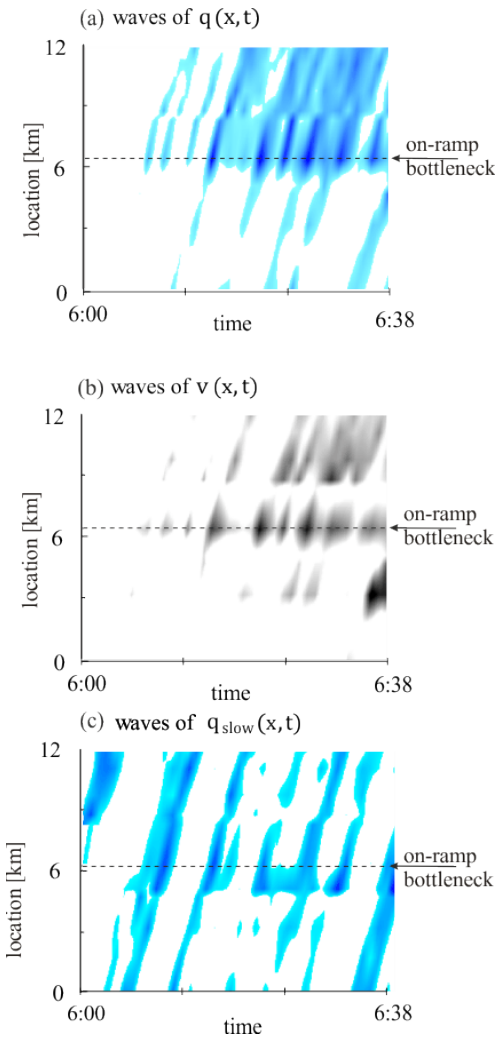

FIG. 2: Empirical waves in free flow shown for time interval $06:00 \le t \le 06:38$ before traffic breakdown has occurred at $t = 06:39$. Real field traffic data measured by road detectors on April 15, 1996 (Monday) (Fig. 1 (b)): (a) Waves of the total flow rate $q(x,t)$ presented by regions with variable shades of gray (blue in the on-line version) (in white regions $q \le 5400$ vehicles/h, in black (dark blue) regions $q \ge 8000$ vehicles/h). (b) Waves of the speed $v(x,t)$ averaged across the road presented by regions with variable shades of gray (in white regions $v \ge 100$ km/h, in black regions $v \le 75$ km/h). (c) Waves of the total flow rate of long vehicles $q_{\rm slow}(x,t)$ presented by regions with variable shades of gray (blue in the on-line version) (in white regions $q_{\rm slow} \le 720$ vehicles/h, in black (dark blue) regions $q_{\rm slow} \ge 1500$ vehicles/h). In formula (4), we use $v_{\rm d} = 90$ km/h, number of virtual road locations $K = 65$ between each pair of detectors, number of virtual time steps within 1 min time interval between two consequent measurements at road detectors is equal to 14.

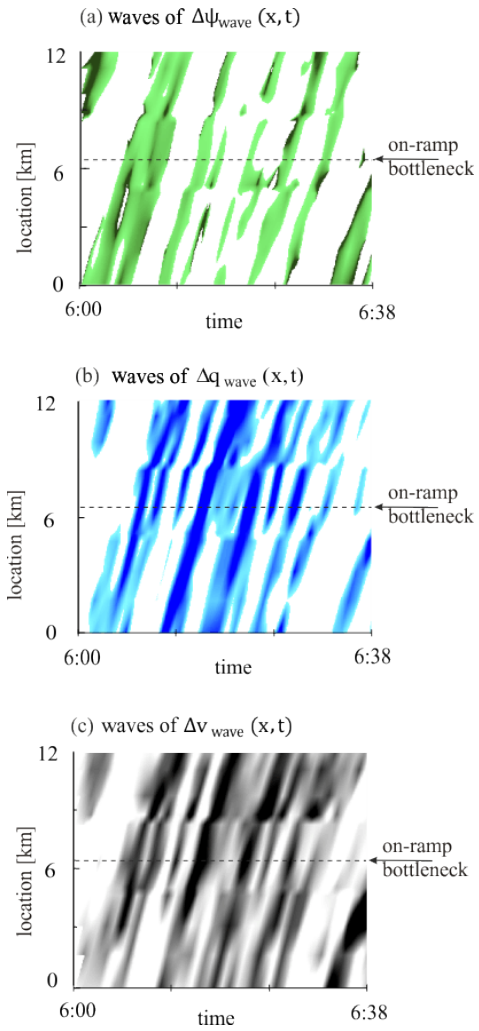

FIG. 3: Empirical waves of $\Delta\psi_{\rm wave}$ (a), $\Delta q_{\rm wave}$ (b), and $\Delta v_{\rm wave}$ (c) for data in Fig. 1 (b) averaged across the road for the same time interval as that in Fig. 2 (real field traffic data measured by road detectors installed along three-lane freeway): (a) Waves of $\Delta\psi_{\rm wave}(x,t)$ are presented by regions with variable shades of gray (green in the on-line version) (in white regions $\Delta\psi_{\rm wave} \leq 0.1$ %, in black (dark green) regions $\Delta\psi_{\rm wave} \geq 1$ %). (b) Waves of $\Delta q_{\rm wave}(x,t)$ are presented by regions with variable shades of gray (blue in the on-line version) (in white regions $\Delta q_{\rm wave} \leq 600$ vehicles/h, in black (dark blue) regions $\Delta q_{\rm wave} \geq 1500$ vehicles/h). (c) Waves of $\Delta v_{\rm wave}(x,t)$ are presented by regions with variable shades of gray (in white regions $\Delta v_{\rm wave} \leq 1$ km/h, in black regions $\Delta v_{\rm wave} \geq 15$ km/h). Model parameters in formula (4) are the same as those in Fig. 2.

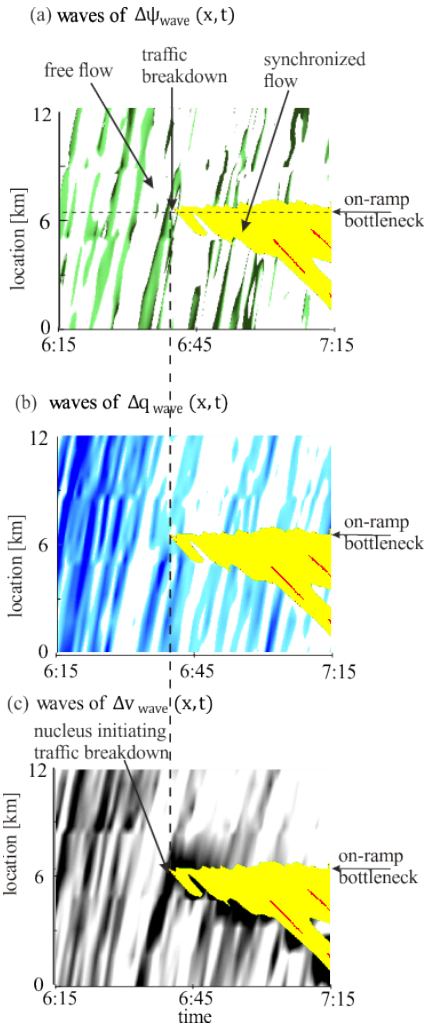

FIG. 4: Empirical nucleus in free flow for data in Fig. 1 (b). Empirical waves of $\Delta\psi_{\rm wave}$ (a), $\Delta q_{\rm wave}$ (b), and $\Delta v_{\rm wave}$ (c) in free flow for a longer time interval as that in Fig. 3 (real field traffic data measured by road detectors installed along three-lane freeway). In (a–c), regions labeled by "synchronized flow" show symbolically synchronized flow. Parameters of the presentation of empirical waves in (a–c) are the same as those in Fig. 3(a–c), respectively.

an off-ramp bottleneck. In Fig. 5, there are three bottlenecks: an off-ramp bottleneck and two upstream on-ramp bottlenecks. In this case, traffic breakdown occurs at the off-ramp bottleneck. This traffic breakdown leads to the emergence of a complex spatiotemporal congested pattern upstream of the off-ramp bottleneck (Fig. 5).

Before the breakdown has occurred, there is also a complex sequence of waves of traffic variables $\Delta\psi_{\rm wave}$, $\Delta q_{\rm wave}$, and $\Delta v_{\rm wave}$ in free flow; some of the waves propagate through the whole 25 km long highway section (Fig. 6).

When we consider a longer time interval as that shown in Fig. 6, we find that while one of the waves approaches the off-ramp bottleneck, the wave initiates traffic breakdown at the bottleneck (Fig. 7). The structure of the wave and its features do not change after the wave is downstream of the off-ramp bottleneck. Thus, as in the

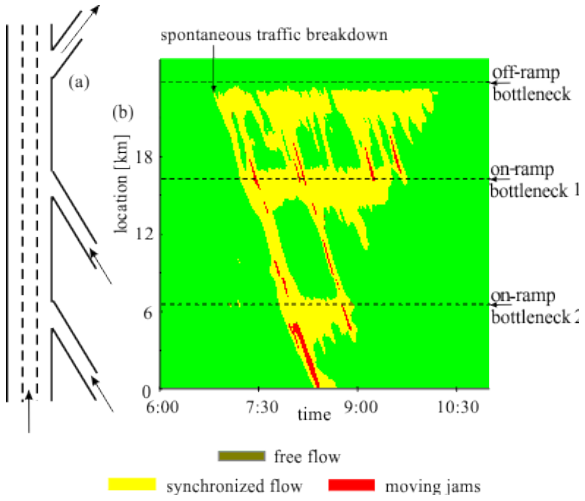

FIG. 5: Overview of empirical features of traffic breakdown (F→S transition) at off-ramp bottleneck: (a) Sketch of section of three-lane freeway A5-South in Germany with off-ramp bottleneck and two upstream on-ramp bottlenecks. (b) Speed data measured with road detectors installed along road section in (a); data is presented in space and time with averaging method described in Sec. C.2 of [17]. Real field traffic data measured by road detectors on September 03, 1998 (Thursday). Off-ramp bottleneck, on-ramp bottleneck 1 and on-ramp bottleneck 2 marked by dashed lines are, respectively, effective bottlenecks B_1, B_2, and B_3 explained in detailed in Sec. 9.2.1 of [14]. Road detectors are at locations: $x = 0$, 1.7, 3.2, 4.7, 5.1, 6.4, 7.9, 8.8, 9.8, 11.1, 12.2, 13.7, 14.8, 15.5, 16.1, 17.0, 17.7, 18.9, 19.8, 20.8, 21.7, 22.8, 23.3, 24.0 km. The on-ramp bottleneck labeled by "on-ramp bottleneck 2" in (b) is the same as that in Fig. 1.

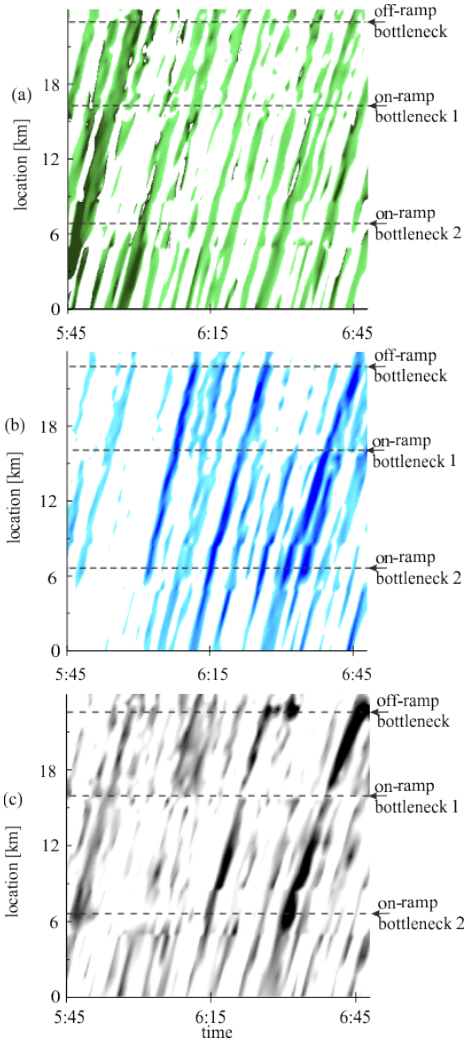

FIG. 6: Empirical waves in free flow averaged across the road, which are associated with data in Fig. 5 (b), for time interval $05:45 \le t \le 06:45$ before the breakdown has occurred: (a) Waves of $\Delta\psi_{\rm wave}$ are presented by regions with variable shades of gray (green in the on-line version) (in white regions $\Delta\psi_{\rm wave} \le 0.1$ %, in black (dark green) regions $\Delta\psi_{\rm wave} \ge 1$ %). (b) Waves of $\Delta q_{\rm wave}$ are presented by regions with variable shades of gray (blue in the on-line version) (in white regions $\Delta q_{\rm wave} \le 700$ vehicles/h, in black (dark blue) regions $\Delta q_{\rm wave} \ge 2000$ vehicles/h). (c) Waves of $\Delta v_{\rm wave}$ are presented by regions with variable shades of gray (in white regions $\Delta v_{\rm wave} \le 2$ km/h, in black regions $\Delta v_{\rm wave} \ge 15$ km/h). Real field traffic data measured on September 03, 1998. Model parameters in formula (4) are the same as those in Fig. 2.

case of the on-ramp bottleneck (Fig. 4 (c)), the wave in free flow mentioned above becomes to be a nucleus for traffic breakdown at the off-ramp bottleneck, when the wave propagates through this bottleneck (Fig. 7 (c)).

D. Empirical probability of spontaneous traffic breakdown at highway bottlenecks

In 1998, Persaud et al. [24] discovered that the empirical probability of traffic breakdown at highway bottlenecks is a growing flow rate function. This empirical probability of traffic breakdown has firstly been explained by an F→S transition in a metastable free flow at an on-ramp bottleneck with the use of simulations of a three-phase cellular automaton model [25]. This theoretical probability of spontaneous breakdown at a highway

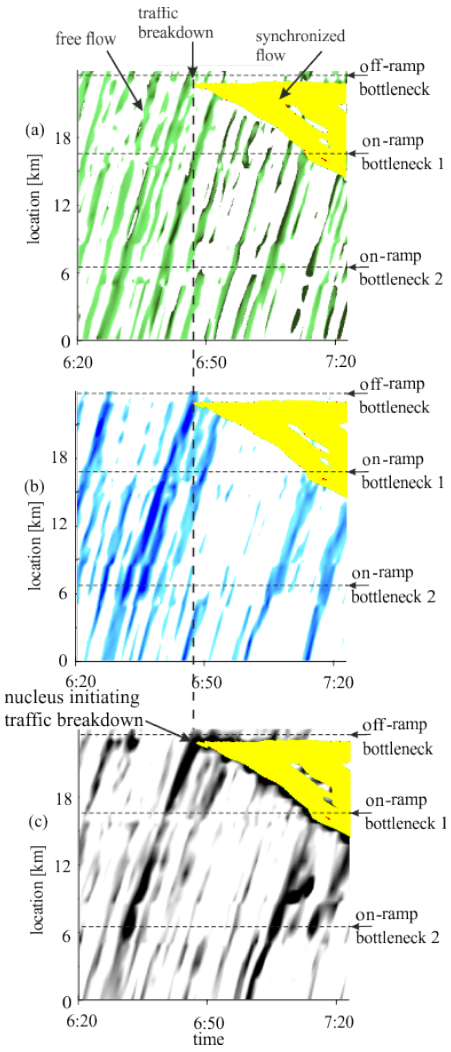

FIG. 7: Empirical nucleus in free flow associated with data in Fig. 5 (b). Empirical waves of $\Delta\psi_{\rm wave}$ (a), $\Delta q_{\rm wave}$ (b), and $\Delta v_{\rm wave}$ (c) in free flow averaged across the road for a longer time interval as that shown in Fig. 6. In (a–c), regions labeled by "synchronized flow" show symbolically synchronized flow. Parameters of the presentation of empirical waves in (a–c) are the same as those in Fig. 6(a–c), respectively. Real field traffic data measured by road detectors on September 03, 1998.

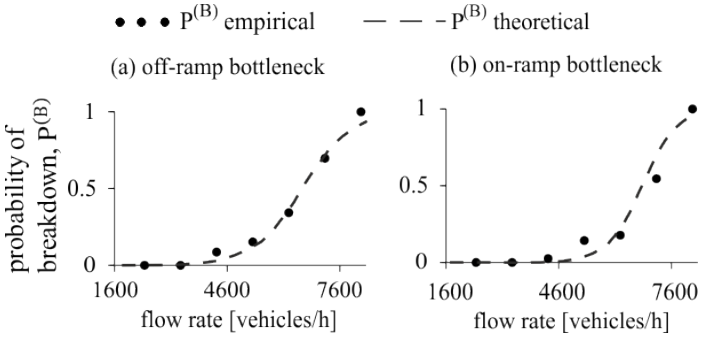

FIG. 8: Comparison of empirical (black points) and theoretical (dashed curves related to (6)) probabilities of traffic breakdown; empirical breakdown probabilities (black points) are related to real field traffic data measured by road detectors installed along a section of three-lane freeway A5-South with effective bottlenecks shown in Fig. 5: (a) Probability of traffic breakdown at on-ramp bottleneck (labeled by "on-ramp bottleneck 1" in Fig. 5 (b)); empirical breakdown probability was found from a study of traffic data in which traffic breakdown was observed on 56 different days. (b) Probability of traffic breakdown at off-ramp bottleneck (labeled by "off-ramp bottleneck" in Fig. 5 (b)); empirical breakdown probability was found from a study of traffic data in which traffic breakdown was observed on 89 different days.

bottleneck is well fitted by a function [25]

$$P^{(\rm B)} = \frac{1}{1+\exp[\alpha(q_{\rm P}-q_{\rm sum})]}, \qquad (6)$$

where $q_{\rm sum}$ is the flow rate in free flow at the bottleneck, α and $q_{\rm P}$ are parameters. Qualitatively the same growing flow-rate function for the breakdown probability has also been found in measured 5-minutes average traffic data [26–30].

However, the wave duration in the data is usually less than 5 minutes (Figs. 2–4, 6 and 7). Therefore, in 5-minutes average traffic data studied in [26–30] the waves cannot usually be resolved.

We study the flow rate functions of the empirical probability of spontaneous traffic breakdown whose nucleation is associated with wave propagation through highway bottlenecks. To find the empirical breakdown probability (black points in Fig. 8), we study data sets of 1-min averaged data measured during in 1996–2014. In each of

the data sets traffic breakdown has been observed. The data sets have been measured on the same section of the freeway A5-South as the data studied above (Figs. 2–7).

Empirical breakdown probabilities (black points in Fig. 8) are found as functions of the total flow rate across the road as follows: (i) The breakdown is measured at detector with the use of 1-min averaged data. In the most of the data sets used for the calculation of the empirical breakdown probability (black points in Fig. 8), a nucleus for traffic breakdown appears during the propagation of one of the waves through the bottleneck location. (ii) The flow rates in free flow (before the breakdown) have been averaged over 15 min intervals. (iii) The flow rate axis is divided in flow rate intervals $(q_k,\ q_k + \Delta q_k)$ with constant $\Delta q_k = 940$ vehicles/h ("k-flow rate interval"), $k = 1, 2, ...K$, where K is the total number of different k-flow rate intervals in free flow; (iv) for each of the k-flow rate intervals, breakdown probability is equal to n_k/N_k, where N_k is the number of observed flow rates within the k-flow rate interval in all data sets, n_k is the number of breakdowns found in the k-flow rate interval.

We have found that the empirical probabilities of traffic breakdown measured at detector as function of the flow rate (black points in Fig. 8) for both the on-ramp and off-ramp bottlenecks are well fitted with a theoretical one given by formula (6) with fitting parameters $(q_{\rm p},\ \alpha^{-1}) =$ (6800, 456) vehicles/h for the on-ramp bottleneck (Fig. 8 (a)) and (6600, 643) vehicles/h for the off-ramp bottleneck (Fig. 8 (b)).

E. Empirical permanent disturbances at highway bottlenecks and nucleation of empirical traffic breakdown

In empirical data sets, a wave moving in free flow at the velocity (5) acts as a nucleus for traffic breakdown *only* at some effective location of a highway bottleneck: No traffic breakdown has been observed between the bottleneck locations. To understand this empirical result, rather than waves of $\Delta v_{\rm wave}$ (Fig. 6), we consider empirical waves of the speed $v(x,t)$ averaged across the road (Fig. 9 (a)).

We see that additionally to waves of the speed propagating downstream, there are three narrow road regions, which are localized in neighborhoods of the locations of off-ramp bottleneck, on-ramp bottleneck 1, and on-ramp bottleneck 2, respectively. Within these narrow regions, the speed is smaller than outside them (Fig. 9 (a)). These narrow regions of the decrease in the speed at the effective locations of the bottlenecks can be called permanent empirical local speed disturbances in free flow at highway bottlenecks [31].

Empirical observations show that a wave acts as a nucleus for traffic breakdown only when the wave reaches the location of a permanent local speed disturbance in free flow at a highway bottleneck. For this reason, the location of the permanent disturbance determines the ef-

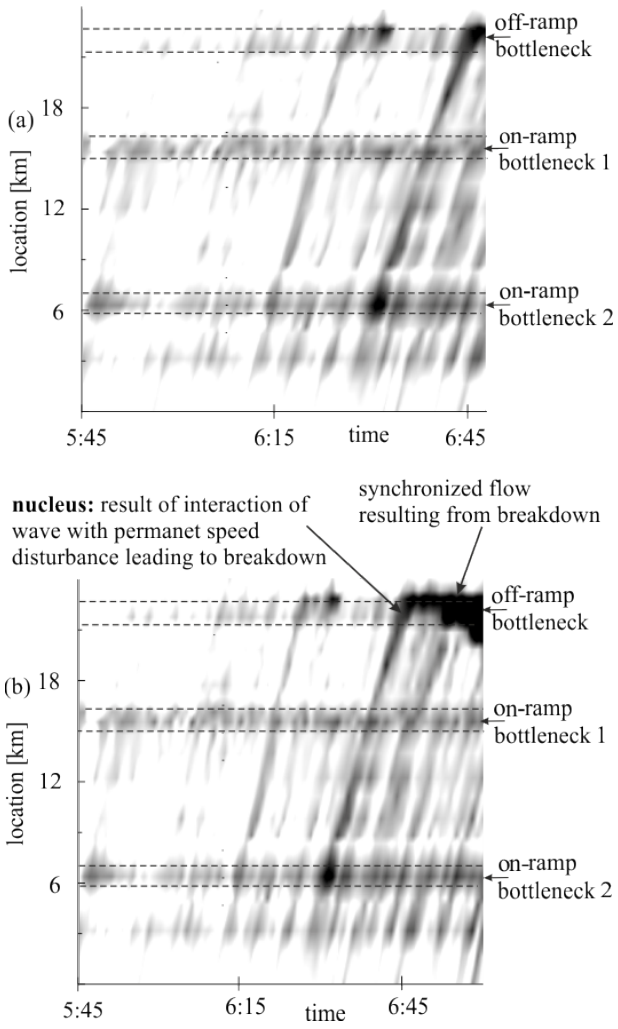

FIG. 9: Explanation of physics of nuclei for traffic breakdown with empirical data: (a) Empirical permanent local speed disturbances in free flow at highway bottlenecks for the data set for which traffic breakdown is shown in Fig. 7 (real field traffic data measured on September 03, 1998). (b) The same data as in (a), however, for a longer time interval showing that the nucleus for the breakdown at the off-ramp bottleneck appears due to some interaction of the wave with a permanent speed disturbance at the bottleneck. In (a, b), empirical data for the speed $v(x,t)$ presented by regions with variable shades of gray; in white regions $v \geq 115$ km/h, in black regions $v \leq 80$ km/h. Parameters of the speed presentation $v(x,t)$ made with (4) are the same as those in Fig. 2. Narrow road regions of a smaller speed (permanent local speed disturbances), which are localized in neighborhoods of the effective locations of the bottlenecks, are marked by double dashed lines. Off-ramp bottleneck, on-ramp bottleneck 1, and on-ramp bottleneck 2 are the same as those in Fig. 6.

fective location of the bottleneck at which traffic breakdown occurs. A decrease in the free flow speed within the permanent local speed disturbance becomes larger, when the wave reaches the effective bottleneck location. This is because within the wave the flow rate is larger and the speed is smaller than outside the wave.

Thus the physics of the occurrence of empirical nuclei for traffic breakdown at highway bottlenecks can be explained by an interaction of a wave in free flow with a permanent speed disturbance localized at the effective location of the bottleneck.

Empirical results presented in Figs. 9 (b) and 10 for the off-ramp bottleneck confirm the above conclusion that a wave becomes to be nucleus for traffic breakdown *only* at the effective locations of the bottleneck at which permanent speed disturbance is localized (Fig. 9 (a)) [32]. The same conclusion is valid for the on-ramp bottleneck (Fig. 11) that is the bottleneck labeled by "on-ramp bottleneck 2" in Fig. 9. For both off- and on-ramp bottlenecks, a wave, within which the percentage of long vehicles (Figs. 10 (a) and 11(a)) and the flow rate are larger (Figs. 10 (c) and 11(c)) whereas the average speed is lower (Figs. 10 (b) and 11(b)) than outside the wave, becomes to be a nucleus for traffic breakdown only at the effective location of the bottleneck at which a permanent speed disturbance is localized (Fig. 9 (a)).

The empirical evidence of the effect of permanent local speed disturbances in free flow at the effective locations of highway bottlenecks on the breakdown nucleation due to wave propagation revealed in the article confirms the theoretical explanation of an F→S transition made in three-phase theory. In this theory, the assumption about the existence of permanent local speed disturbances in free flow at the effective locations of highway bottlenecks should explain why the probability of the F→S transition in metastable free flow is considerably larger at the bottlenecks than outside them [14, 19–22].

More than 160 traffic breakdowns at on- and off-ramp bottlenecks on different highways in Germany that measured during 1996–2014 have been studied. It turns out that the empirical result of breakdown nucleation at a highway bottleneck due to the interaction of a wave in free flow with a permanent speed disturbance localized at the effective location of the bottleneck is the common one for the most of the data sets.

III. EMPIRICAL SPATIOTEMPORAL STRUCTURE OF NUCLEI AND MICROSCOPIC THEORY OF BREAKDOWN NUCLEATION

A. Empirical two-dimensional (2D) asymmetric spatiotemporal structure of nuclei for traffic breakdown

To study a possible effect of a non-homogeneity of traffic flow across the road on the breakdown nucleation, we consider empirical traffic variables in different freeway lanes (Figs. 12 and 13). We should mention that the most of long vehicles move in the right lane (sometimes traffic flow in the right lane consists of almost 100% (slow) long vehicles) (Fig. 12 (a)). The percentage of long vehicles ψ in the middle lane is considerably smaller than in the right lane; almost no long vehicles move in the left lane (Fig. 12 (a)).

We have found the following empirical result: An empirical wave in free flow exhibits a two-dimensional (2D) structure: Wave's characteristics are different in different highway lanes (Fig. 13). This wave structure is asymmetric for different traffic variables in the perpendicularly direction to the flow direction. The most waves of long vehicles are observed in the right lane, while in the left lane almost no waves of $\Delta\psi_{\text{wave}}$ exist. On contrary, the most waves of the flow rate and vehicle speed are observed in the left lane, while in the right lane almost no waves of Δq_{wave} and Δv_{wave} exist.

However, to understand the effect of 2D asymmetric structure of nuclei on features of traffic breakdown, a study of *microscopic* empirical data is required in which lane changing and vehicle acceleration (deceleration) in a neighborhood of a bottleneck can be resolved. Unfortunately, such microscopic (single-vehicle) empirical data for free flow at bottlenecks is currently not available. Therefore, in Sec. III B with the use of a three-phase stochastic microscopic traffic flow model, we study theoretical predictions about the effect of 2D asymmetric structure of nuclei on microscopic features of traffic breakdown at an on-ramp bottleneck.

B. Microscopic theory of the nucleation of traffic breakdown at highway bottlenecks

1. Model

We consider a simple model of traffic flow on two-lane road with an on-ramp bottleneck. In this model, we assume that traffic flow consists of identical passenger vehicles in which there is only one slow vehicle moving in the right road lane. Such a model of traffic flow with a slow vehicle is known as a "moving bottleneck" model [35–44].

However, as explained in details in [16], traffic flow models used in [35–43] cannot describe an F→S transition in metastable free flow at a highway bottleneck, as observed in all known measured traffic data [14] including empirical field traffic data studied in this article. Therefore, we make simulations with a stochastic microscopic three-phase traffic flow model with on-ramp and moving bottlenecks of Ref. [44]. In this model, states of synchronized flow cover a two-dimensional region (2D) in the flow–density plane (Fig. 14 (a)), as it follows from a hypothesis of three-phase theory about states of synchronized flow [45–47]. As shown in [23, 44, 50–52], this model can reproduce all known empirical macroscopic features of traffic breakdown (F→S transition) in metastable free flow at highway bottlenecks [53].

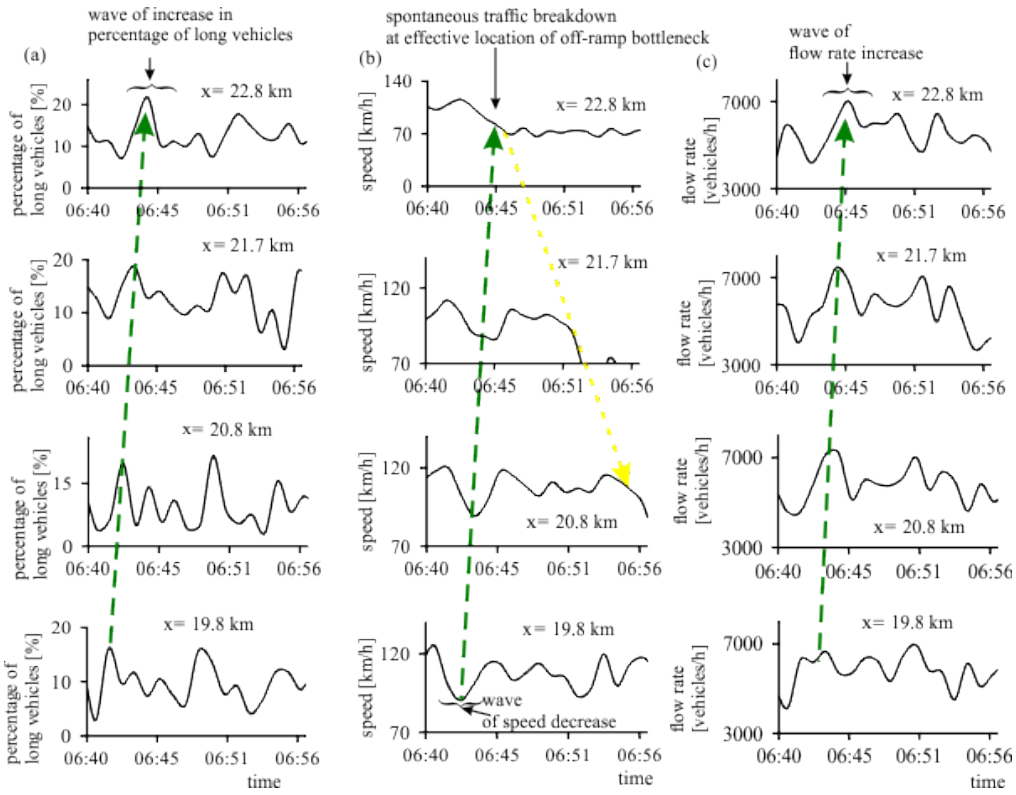

FIG. 10: Empirical time-distributions of traffic variables averaged across the road at different detector locations within a wave that initiates the breakdown at the location of a permanent speed disturbance (effective location of the off-ramp bottleneck): (a) The percentage of long vehicles. (b) The speed. (c) The total flow rate. Arrows in downstream direction show regions of the downstream propagation of the wave. The arrow in upstream direction in (b) shows the propagation of synchronized flow that has occurred due to the breakdown at the off-ramp bottleneck. The same real field traffic data as that shown in Fig. 7.

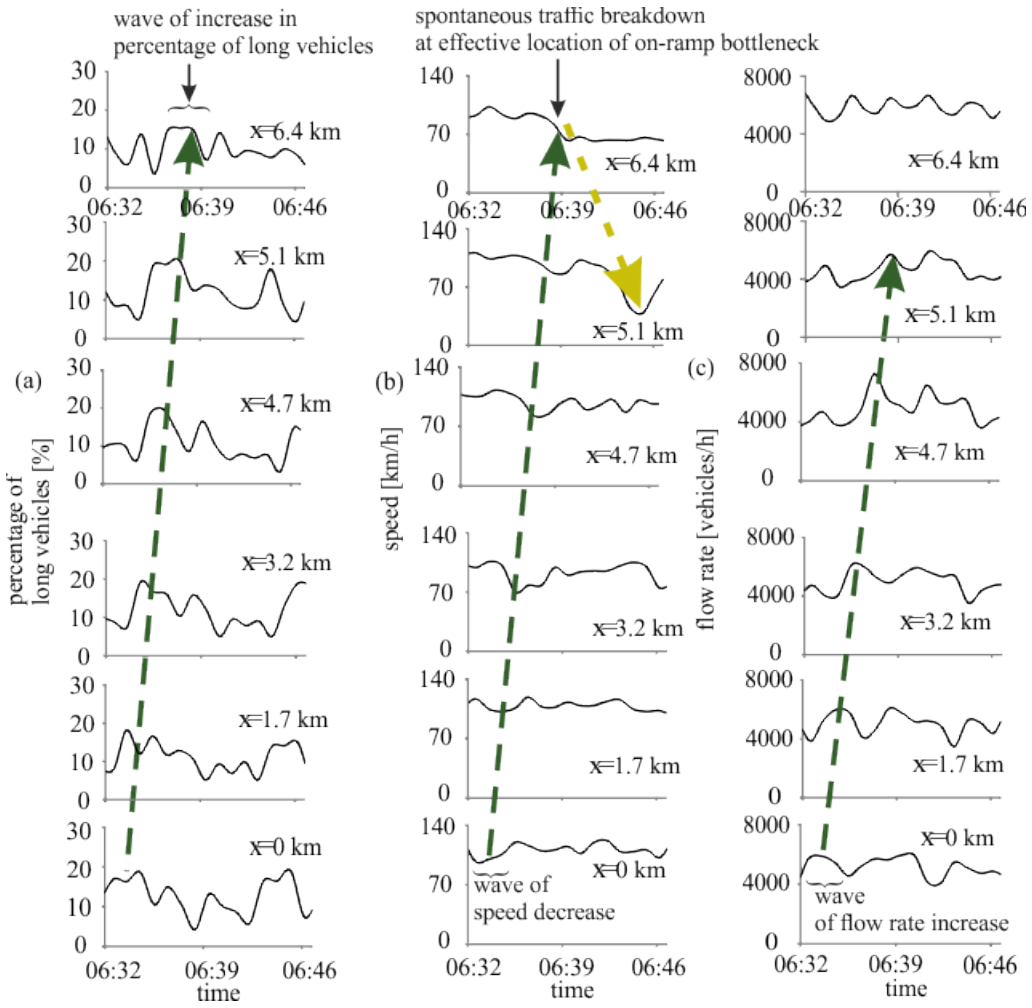

FIG. 11: Empirical time-distributions of traffic variables at different road detector locations within a wave that initiates the breakdown at the on-ramp bottleneck: (a) The percentage of long vehicles. (b) The speed averaged across the road. (c) The total flow rate. Arrows in downstream direction show regions of the downstream propagation of the wave. The arrow in upstream direction in (b) shows the propagation of synchronized flow that has occurred due to the breakdown at the bottleneck. The same real field traffic data as that shown in Figs. 1 (b) and 4 measured on April 15, 1996; the on-ramp bottleneck is the bottleneck labeled by "on-ramp bottleneck 2" in Fig. 9; the effective location of this on-ramp bottleneck is approximately equal to $x = 6.4$ km.

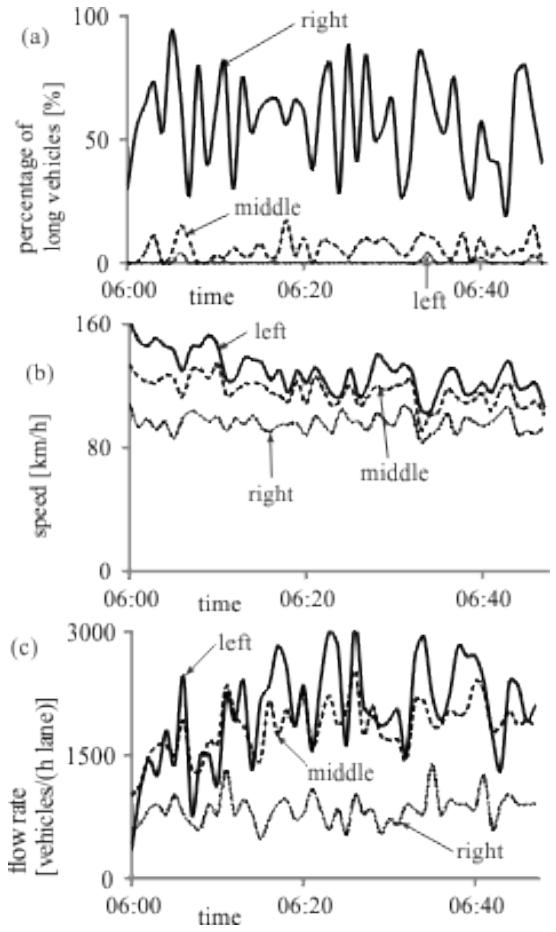

FIG. 12: Empirical time-dependencies of percentage of long vehicles (a), speed (b), and flow rate (c) in different highway lanes at location $x = 0$ km for real field traffic data shown in Fig. 1 (b).

A moving bottleneck is caused by a slow vehicle that moves in the right lane at a maximum speed $v_{\rm M}$ that is lower than the speed of other (identical) vehicles $v_{\rm free}$. It is assumed that there is a road region with length $L_{\rm c}$ upstream of the slow vehicle (Fig. 14 (b)). This region is a *moving* one at the speed $v_{\rm M}$. Within this moving region $L_{\rm c}$, called as "moving merging region" of the moving bottleneck, all passenger vehicles moving in the right lane change to the left lane, while approaching the moving bottleneck; this lane changing occurs independent of the speed difference between lanes, when some safety conditions are satisfied (Sec. A 2). The length $L_{\rm c}$ of the moving merging region is associated with the mean distance at which vehicles recognize the slow vehicle. In accordance with [44], a moving bottleneck can be a nucleus for traffic breakdown (F→S transition) at an on-ramp bottleneck (Fig. 14 (c)). Because the rules of vehicular motion in the three-phase traffic flow model as well as in the bottleneck models (Fig. 14 (b)) have been presented and discussed in details in [44], they are given in Appendix A.

2. *Microscopic 2D asymmetric structure of waves in free flow*

To understand the 2D asymmetric structure of empirical waves in free flow (Sec. III A) as well as a possible impact of this wave structure on traffic breakdown, in comparison with [44], we study here the effect of the moving bottleneck on spatiotemporal distributions of traffic variables in different road lanes (Fig. 14 (d–g)), on lane changing behavior in a neighborhood of the moving bottleneck upstream of the on-ramp bottleneck (Fig. 15) and in a neighborhood of the on-ramp bottleneck (Fig. 16).

To pass the slow vehicle (moving bottleneck), vehicles moving in the right lane change to the left lane within the merging region of the moving bottleneck (up-arrows R→L for vehicles 1 and 2 in Fig. 15). After passing the slow vehicle, most of these vehicle change back to the right lane (down-arrows L→R for vehicles 1 and 2 in Fig. 15). This sequence R→L→R of lane changing leads to an increase in the flow rate in the left lane in a neighborhood of the slow vehicle (Fig. 14 (d)). Therefore, this increase in the flow rate in the left lane moves with the speed of the slow vehicle: A wave of the increase in the flow rate occurs that moves at the velocity $v_{\rm M}$ (Fig. 14 (d)). Due to the increase in the flow rate, the speed in the left lane within the wave decreases. Time-distributions of the flow rate, speed, and density within the wave in the left lane (Fig. 14 (e–g)) confirm these conclusions about the wave features.

There is also an increase in the flow rate in the right lane. This increase in the flow rate is due to an increase in the vehicle density upstream of the moving bottleneck (Fig. 14 (b)); however, this increase in the flow rate is considerably smaller than that in the left lane. Thus the wave of the flow rate exhibits a 2D asymmetric structure whose characteristics are different in different highway lanes (Fig. 14 (d)). This is qualitatively exactly the same effect as observed in real field empirical data (Sec. III A).

These simulations allow us to explain empirical waves in free flow (Secs. II A and III A) as follows. In empirical data, the percentage of slow (long) vehicles in the right lane exhibits large oscillations over time (Fig. 12(a)). Therefore, waves of slow vehicles occur in the right lane. Because the most of slow vehicles move in the right lane (Fig. 12 (a)), the largest wave amplitude $\Delta\psi_{\rm wave}$ is observed in the right lane (left column in Fig. 13 (a)), whereas almost no waves of slow vehicles is observed in the left lane (left column in Fig. 13 (c)) [107].

There are very different empirical vehicle speeds in the left and middle lanes (Fig. 12(b)). This allows us to assume that there are passenger vehicles that prefer the

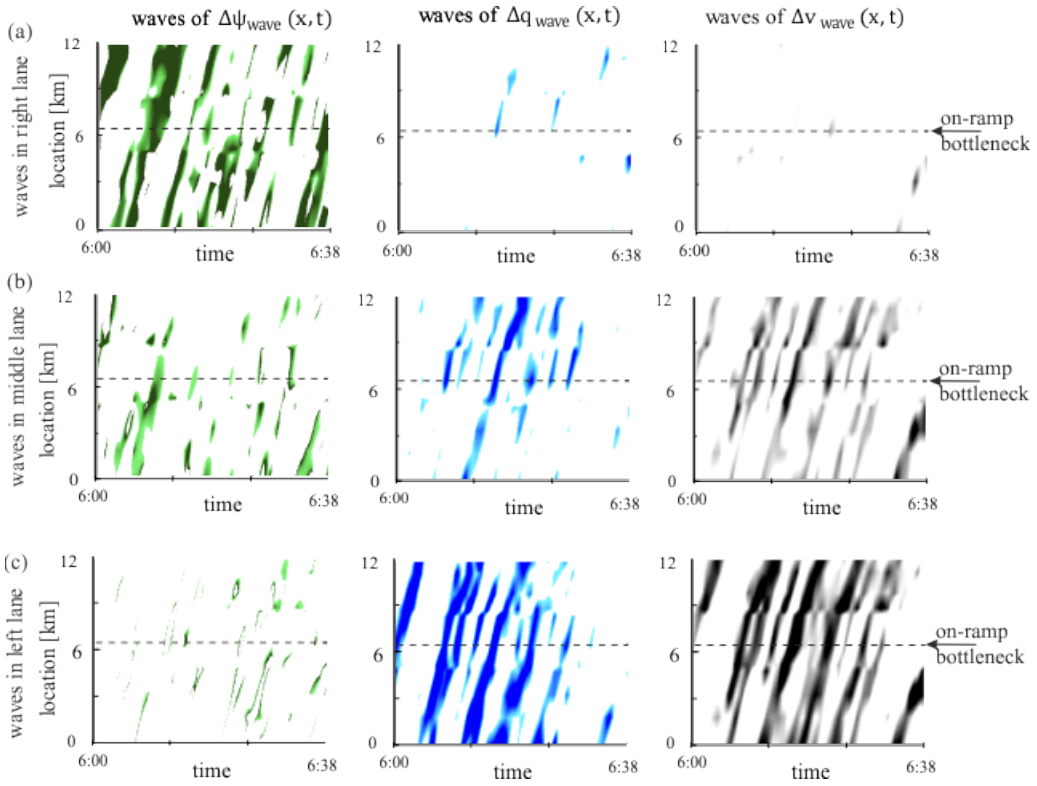

FIG. 13: Empirical waves of the percentage of slow (long) vehicles $\Delta\psi_{\rm wave}$ (left column), the flow rate $\Delta q_{\rm wave}$ (middle column), and the vehicle speed $\Delta v_{\rm wave}$ (right column) in free flow for different road lanes for real field traffic data shown in Fig. 1 (b) during the same time interval as that in Fig. 2: (a) Right lane. (b) Middle lane. (c) Left lane. Waves of $\Delta\psi_{\rm wave}(x,t)$ are presented by regions with variable shades of gray (green in the on-line version) (in white regions $\Delta\psi_{\rm wave} \leq 0.3$ %, in black (dark green) regions $\Delta\psi_{\rm wave} \geq 1$ %). Waves of $\Delta q_{\rm wave}(x,t)$ are presented by regions with variable shades of gray (blue in the on-line version) (in white regions $\Delta q_{\rm wave} \leq 480$ vehicles/h, in black (dark blue) regions $\Delta q_{\rm wave} \geq 800$ vehicles/h). Waves of $\Delta v_{\rm wave}(x,t)$ are presented by regions with variable shades of gray (in white regions $\Delta v_{\rm wave} \leq 7$ km/h, in black regions $\Delta v_{\rm wave} \geq 20$ km/h). Model parameters in formula (4) are the same as those in Fig. 2.

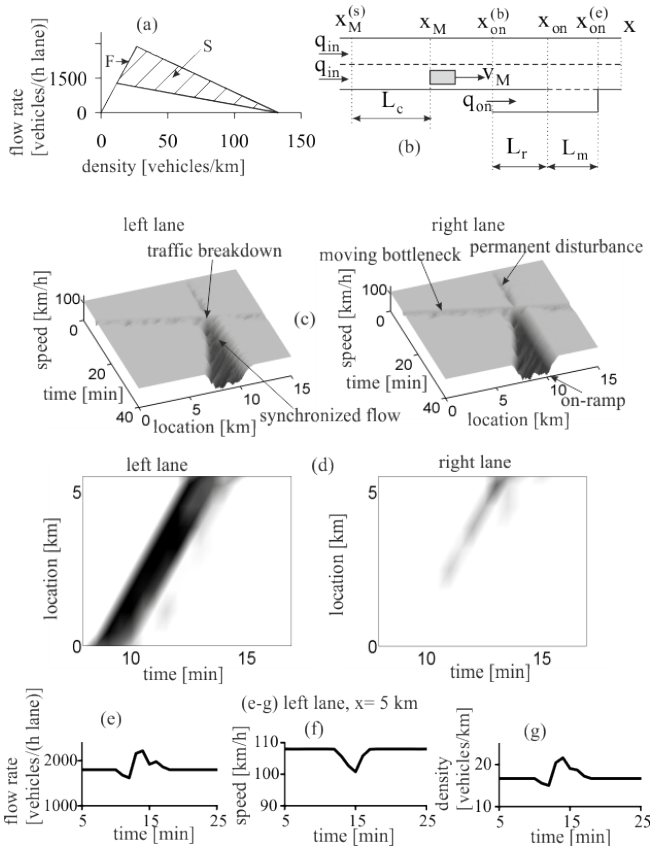

FIG. 14: Simulations of the nucleation of traffic breakdown on two-lane road with on-ramp bottleneck through wave propagation in free flow: (a) Hypothesis of three-phase theory about 2D-steady states of synchronized flow incorporated in a stochastic microscopic three-phase model used for simulations. (b) Models of moving and on-ramp bottlenecks. (c) Nucleation of traffic breakdown at on-ramp bottleneck through wave propagation caused by a moving bottleneck in different road lanes (left – left lane, right – right lane). (d) Wave of the flow rate $q(x,t)$ in different road lanes (left – left lane, right – right lane) presented by regions with variable shades of gray (in white regions $q \leq 2000$ vehicles/h, in black regions $q \geq 2150$ vehicles/h); wave presentation is made with the use of a virtual detector moving at the speed $v_{\rm M}$ (Appendix B). (e–g) Time-functions of the flow rate (e), the speed (f) and the density (g) within the wave in the left lane at location $x =$ 5 km. $v_{\rm M} = 82.8$ km/h, $(q_{\rm in},\ q_{\rm on}) = (1800,\ 750)$ vehicles/h, $x_{\rm on} = 10$ km. Other model parameters are in Table III of Appendix A.

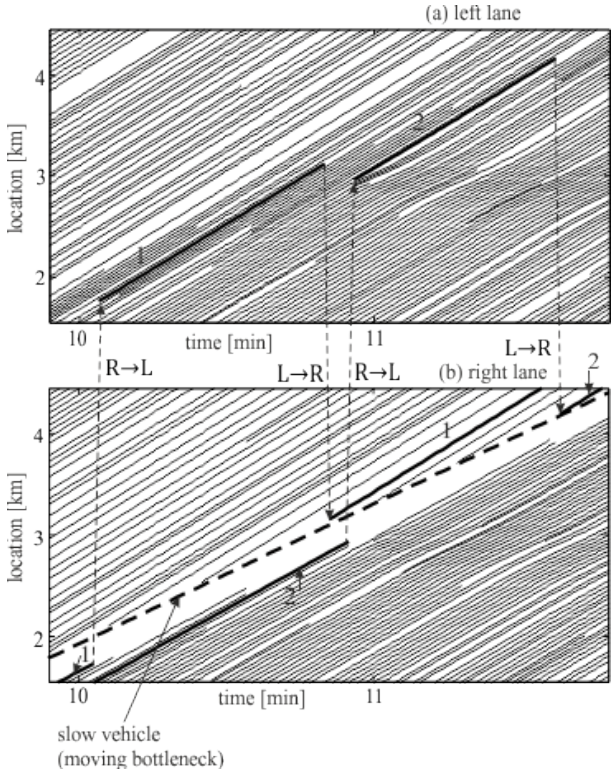

FIG. 15: Fragment of simulated vehicle trajectories of sequence R→L→R of lane changing in a neighborhood of the slow vehicle (moving bottleneck) associated with simulations shown in Fig. 14 (c, d): (a) Left lane. (b) Right lane.

uninterrupted motion at a higher speed in the left lane, and those passenger vehicles that prefer the motion in the middle and right lanes at a lower speed, while using the left lane for passing only.

We can assume that the frequency of this passing increases considerably when passenger vehicles approach a wave of slow vehicles in the right lane: The passenger vehicles change firstly to the left lane and, after the vehicles have passed the wave, they change back to the middle and to the right lanes. This is qualitatively the same effect as the sequence R→L→R of lane changing in the neighborhood of the slow vehicle found in simulations (Fig. 15).

Thus, during the passing of a wave of slow vehicles in the right lane, the flow rate in the left lane increases firstly, and then the flow rate decreases. As in simulations (Fig. 14 (d)), this should lead to the wave of the flow rate in the left lane caused by the wave of slow vehicles in the right lane (Fig. 13). This explains the emergence of waves $\Delta q_{\rm wave}$ moving at the average speed of slow vehicles (5) (Figs. 3 and 13) that is considerably smaller than the vehicle speed in the left and middle lanes (Fig. 12). As in simulations, the increase of the flow rate in free flow leads to a speed decrease; therefore, as in simulations (Figs. 14 (e, f)), in empirical observations a 2D-structure of the

waves of the speed and flow rate coincide qualitatively each other (middle and right columns in Fig. 13).

3. *Microscopic structure of permanent speed disturbance at bottleneck*

In simulations, there is a permanent speed disturbance at the on-ramp bottleneck (Fig. 16). To explain the disturbance, note when the flow rate $q_{\rm in}$ (Fig. 14 (b)) is large enough, due to vehicle merging from the on-ramp into the right lane of the main road (vehicle "p" in Fig. 16 (a)), the following vehicle moving in the right lane on the main road decelerates (vehicle 3 in Fig. 16 (a–c)). This deceleration of vehicle 3 forces the following vehicles 4 and 5 to decelerate: The speed disturbance occurs in a neighborhood of the merging region on the on-ramp ($x_{\rm on} \le x \le x_{\rm on}^{\rm (e)}$ in Figs. 14 (b) and 16 (a–c)). Although the minimum speed within the disturbance increases over time (vehicle 3–5 in Fig. 16 (b, c)), the disturbance is maintained on average because next vehicle that merges from the on-ramp onto the main road (vehicle "m" in Fig. 16 (a)) leads to the deceleration of the following vehicle (vehicle 6 in Fig. 16 (a–c)), and so on.

The permanent speed disturbance occurs also in the left lane (vehicle 7 in Fig. 16 (d–f)). The disturbance appears due to vehicles that decelerate initially within the disturbance in the right lane and then they change to the left lane as shown with an example of vehicle 8 together with arrow labeled by R→L in Fig. 16 (a, d). Due to this lane changing, the following vehicle 9 must decelerate to a smaller speed than that of vehicle 8. The lane changing maintains the permanent speed disturbance in the left lane (vehicles 9–11 in Fig. 16 (d–f)).

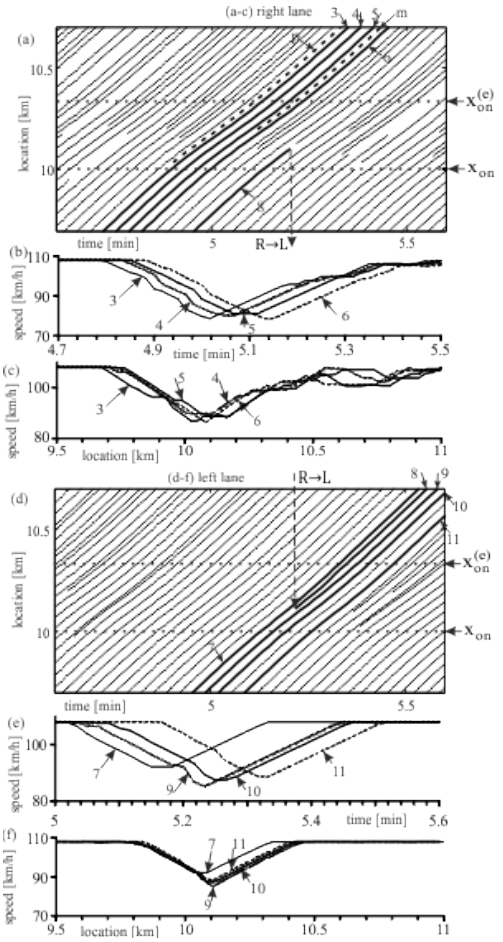

FIG. 16: Simulations of permanent local disturbance in free flow at on-ramp bottleneck associated with Fig. 14 (c): (a–c) Fragment of vehicle trajectories (a) and microscopic (single-vehicle) speed along chosen trajectories (b, c) in time (b) and location (c) whose numbers are the same in (a) and (b, c) in the right lane. (d–f) Fragment of vehicle trajectories (d) and microscopic speed along chosen trajectories (e, f) in time (e) and location (f) whose numbers are the same in (d) and (e, f) in the left lane.

4. *Microscopic features of interaction of waves in free flow with permanent local disturbance at bottleneck*

Before the moving bottleneck reaches the on-ramp bottleneck, no spontaneous traffic breakdown occurs at the on-ramp regardless of the existence the permanent speed disturbance. This is because at chosen flow rates $q_{\rm in}$ and $q_{\rm on}$ the probability of spontaneous traffic breakdown due to model fluctuations is small (although this probability is larger than zero). However, when the wave reaches the effective location of the on-ramp bottleneck (Fig. 14 (c)), the speed decreases at the bottleneck additionally to that within the permanent speed disturbance; as a result, the wave becomes to be a nucleus for spontaneous traffic breakdown at the bottleneck.

In simulations, this traffic breakdown is associated with the interaction of the permanent speed disturbance with the wave of the flow rate and speed caused by the moving bottleneck. The breakdown begins to develop in the left lane in which the flow rate is larger and the speed is smaller than outside the wave. Firstly, within the region of the permanent disturbance ($x_{\rm on} \le x \le x_{\rm on}^{\rm (e)}$ in Figs. 14 (b) and 17), vehicle "p2" merges from the on-ramp into the right lane; this vehicle changes quickly to the left lane (up-arrow R→L for vehicle "p2" in Fig. 17). Due to the increase in the flow rate within the wave in the left lane, following vehicles 12–14 should decelerate. This vehicle deceleration causes traffic breakdown: the upstream front of synchronized flow is forming in the left lane while propagating upstream (dotted-dashed line labeled by F→S in Fig. 17 (a)). Vehicles 15 and 16 approaching this front of synchronized flow change to the right lane (down-arrows L→R for vehicles 15 and 16 in Fig. 17). However, vehicles 15 and 16 should follow vehicle "m2" that has just merged from the on-ramp into the right lane. Thus vehicles 15 and 16 should decelerate. This vehicle deceleration causes traffic breakdown:

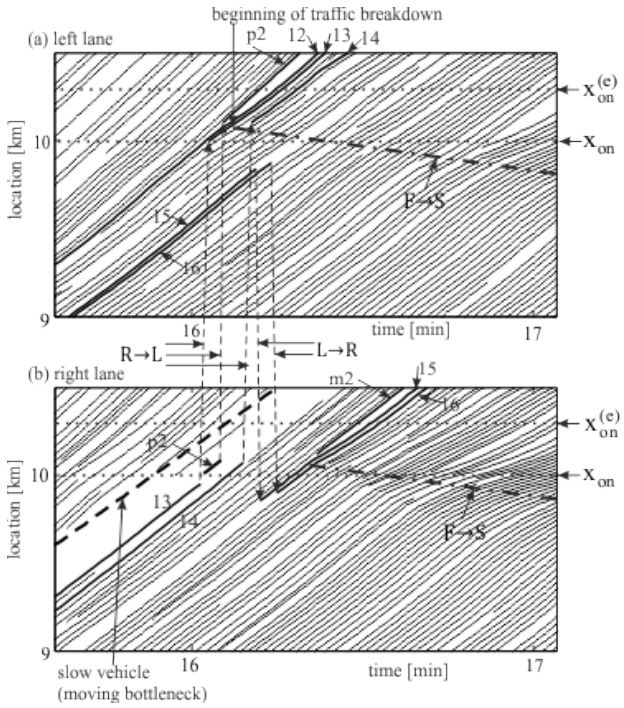

FIG. 17: Fragments of simulated vehicle trajectories associated with Fig. 14 (c): (a) Left lane. (b) Right lane.

the upstream front of synchronized flow is forming in the right lane while propagating upstream (dotted-dashed line labeled by F→S in Fig. 17 (b)).

In contrast to simulations with a single slow vehicle (Fig. 14 (b)), in real field data there are many slow vehicles (Secs. II and III A). However, in the empirical data there are large time-oscillations of the percentage of slow vehicles (Fig. 12 (a)). For this reason, a sequence of waves of slow vehicles occurs (left column in Fig. 13). Based on a simple model with the single slow vehicle, we have simulated one of such waves of real traffic (Figs. 14–17). We have found that, as in empirical observations (Fig. 13), in simulations the wave exhibits a 2D-structure of the flow rate and speed (Fig. 14 (d–f)). Moreover, as in empirical observations (Sec. II), in simulations we have found that a nucleus for traffic breakdown (F→S transition) at the bottleneck (Figs. 14 (c) and 17) occurs due to an interaction of this wave with a permanent speed disturbance at a highway bottleneck. Thus the above simulations can (at least qualitatively) explain the physics of empirical findings of Secs. II and III A.

IV. DISCUSSION

A. Sources of nucleus for empirical traffic breakdown

Both an empirical wave in free flow (Figs. 1 (b) and 4) and a localized congested pattern (wide moving jam in Fig. 1 (c)) become to be nuclei for traffic breakdown, when they reach the effective location of a highway bottleneck. However, the propagation of a single congested pattern to the effective bottleneck location is sufficient for the inducing of the breakdown at the bottleneck. In contrast, many waves in free flow can propagate through the bottleneck while initiating no breakdown at the bottleneck (Figs. 3 and 6).

The latter empirical result allows us to assume that at a given flow rate in free flow at a highway bottleneck there is a *critical wave* related to a *critical nucleus* for traffic breakdown. Therefore, if a wave is a smaller one than the critical wave for a given flow rate at a highway bottleneck, then no breakdown occurs while the wave propagates through the bottleneck. For example, all waves shown in Fig. 3 for $t < 6:35$ and in Fig. 6 for $t < 6:40$ should be smaller than critical waves. However, waves that become to be nuclei for the breakdown at the effective locations of the bottlenecks in Figs. 4 and 7 should be equal to or larger ones than critical waves for the breakdown at the related bottlenecks, respectively.

In contrast with waves in free flow, within a congested pattern the speed is usually smaller than a critical speed required for the breakdown in free flow at a bottleneck. For this reason, at the flow rate satisfying condition $q_{\rm sum} > C_{\rm min}$, any localized congested pattern becomes to be a nucleus for traffic breakdown, when the pattern reaches the effective bottleneck location.

Thus a basic difference between *empirical spontaneous* (Fig. 1 (b)) and *empirical induced* breakdowns (Fig. 1 (c)) is as follows: To initiate the spontaneous breakdown at the bottleneck, i.e., to be a nucleus for the breakdown, a wave in free flow should be equal to or a larger one than a critical wave. In contrast, a localized congested pattern is always a nucleus for the breakdown at the bottleneck, when condition $q_{\rm sum} > C_{\rm min}$ is satisfied, i.e., when traffic breakdown can occur at the bottleneck.

However, after the breakdown has occurred, characteristics of a congested pattern that has been formed at the bottleneck do not depend on whether the congested pattern has occurred due to empirical spontaneous breakdown or due to empirical induced breakdown. This statement is illustrated by empirical data presented in Fig. 18. In Fig. 18 (a), a congested pattern at the on-ramp bottleneck (Fig. 1 (b)) has occurred due to empirical spontaneous breakdown caused by a wave that becomes to be a nucleus for the breakdown, when the wave is at the effective bottleneck location (Fig. 4). In contrast, in Fig. 18 (b) a congested pattern at the on-ramp bottleneck (Fig. 1 (c)) has been induced due to the propagation of a wide moving jam through the bottleneck. Empirical

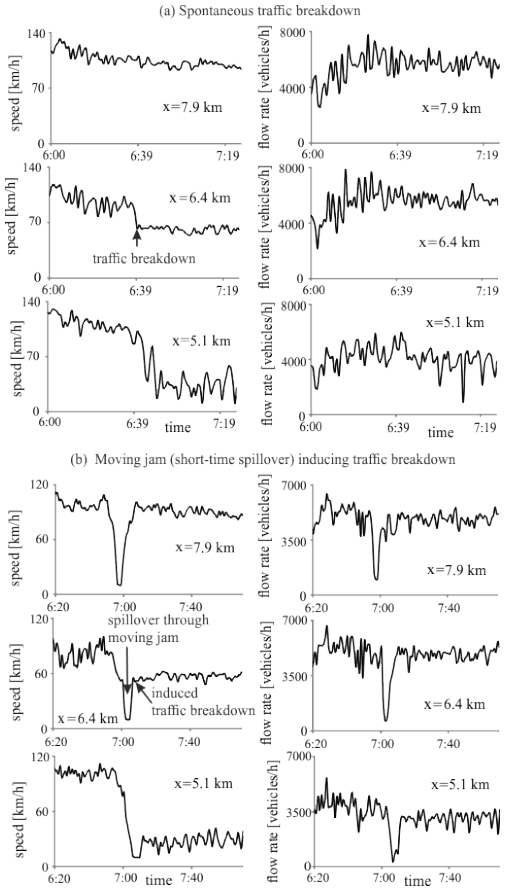

FIG. 18: Empirical 1-min average speed (left column) and flow rate (right column) as time-functions measured by detectors installed on freeway A5-South at the bottleneck location ($x = 6.4$ km), downstream ($x = 7.9$ km) and upstream of the bottleneck ($x = 5.1$ km): (a) Real field traffic data measured on April 15, 1996 (Fig. 1 (b)). (b) Real field traffic data measured on March 22, 2001 (Fig. 1 (c)).

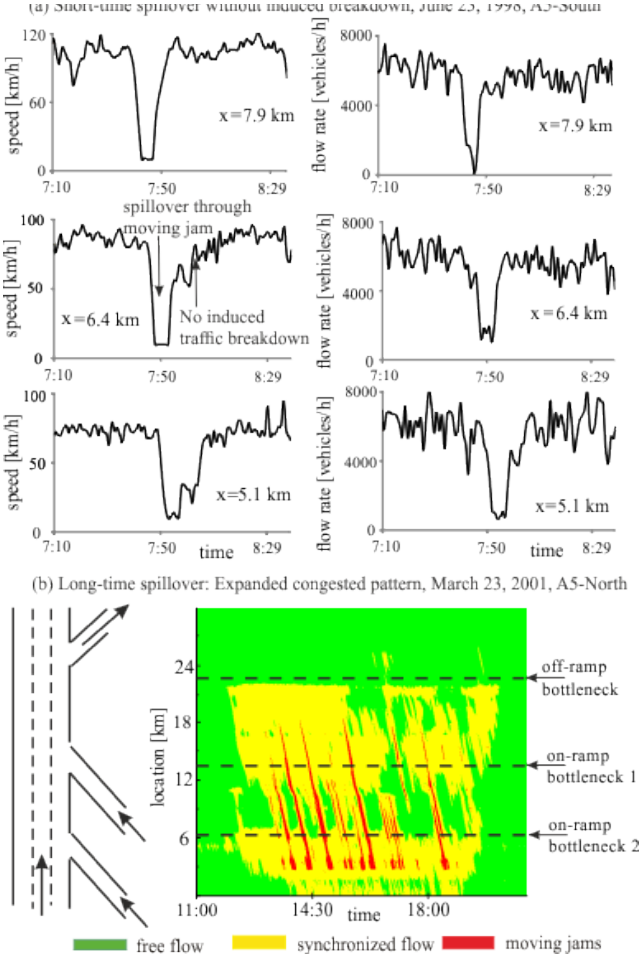

FIG. 19: Empirical examples of spillover without induced traffic breakdown (real field traffic data measured by road detectors on three-lane freeway A5-South (a) and A5-North (b) in Germany): (a) Short-time spillover through moving jam propagation without induced traffic breakdown at on-ramp bottleneck. In (a), empirical 1-min average speed (left column) and flow rate (right column) as time-functions measured by detectors installed on freeway A5-South at the bottleneck location ($x = 6.4$ km), downstream ($x = 7.9$ km) and upstream of the bottleneck ($x = 5.1$ km) are shown; data was measured on June 23, 1998 (Fig. 1 (d)). (b) Long-time spillover leading to expanded congested pattern (right) measured on March 23, 2001 and scheme of freeway section of freeway A5-North with three bottlenecks (left). Bottlenecks in (b) have been explained in Sec. 9.2.2 of [14].

studies show that features of congested traffic resulting from the induced breakdown (at $t > 7{:}07$ in Fig. 1 (c)) are qualitatively identical to those found in congested traffic resulting from empirical spontaneous traffic breakdown (Fig. 1 (b)). In particular, in both cases congested traffic resulting from the breakdown at the bottleneck is self-maintained under free flow conditions downstream of the bottleneck.

This shows that rather than the nature of traffic breakdown, the terms *empirical spontaneous* and *empirical induced* traffic breakdowns at a bottleneck distinguish different *sources* of a nucleus that occurrence leads to traffic breakdown: In Fig. 1 (b), the source of empirical spontaneous breakdown is one of the waves in free flow shown in Fig. 4. In Fig. 1 (c), the source of empirical induced breakdown is the wide moving jam.

In contrast with the wide moving jam shown in Fig. 1 (c), a wide moving jam shown in Fig. 1 (d) does not induce traffic breakdown at the bottleneck. Indeed, in the latter case, after the jam is far away upstream of the bottleneck, free flow returns both at the effective bottleneck location as well as downstream and upstream of the bottleneck (Fig. 19 (a)). Because under condition $q_{\text{sum}} > C_{\text{min}}$ the jam is always a nucleus for traffic breakdown at the bottleneck, the case shown in Fig. 1 (d)

should be related to the opposite condition $q_{\rm sum} < C_{\rm min}$ at which no traffic breakdown can occur at the bottleneck. We see that empirical induced traffic breakdown is probably the only one "method" to find whether traffic breakdown can occur at the bottleneck or not.

This emphasizes another difference between empirical spontaneous and empirical induced traffic breakdowns at a highway bottleneck: When waves in free flow propagate though the bottleneck without initiating of the breakdown, we cannot state whether all waves are smaller than a critical wave, or condition $q_{\rm sum} < C_{\rm min}$ is satisfied at which no traffic breakdown can occur at the bottleneck. In contrast, when a local congested pattern propagates through the bottleneck without inducing of the breakdown, we can state that the flow rate at the bottleneck is smaller than $C_{\rm min}$.

B. Induced traffic breakdown as one of different consequences of spillover in real traffic

The effect of continuous upstream propagation of traffic congestion is often called *spillback*. When due to this upstream propagation a congested pattern affects an upstream road bottleneck, it is often called *spillover*. In the cases of the wide moving jams shown in Figs. 1 (c) and 1 (d), any of the jams can also be considered the effect of spillover because the jam forces congested traffic at the bottleneck.

However, when the jams are far away upstream of the bottleneck, they do not force congested traffic at the bottleneck any more. We can see that there can be at least the following qualitatively different effects due to spillover at a highway bottleneck:

(i) An empirical induced traffic breakdown occurs due to jam propagation through a bottleneck (Fig. 1 (c)).

(ii) An expanded congested pattern (EP) occurs due to spillover (Fig. 19 (b)) [108]: The EP shown in Fig. 19 (b) appears when an empirical congested pattern that occurs initially at an off-ramp bottleneck propagates upstream (spillback). Due to this upstream pattern propagation it forces congested conditions at an upstream on-ramp bottleneck (labeled by "on-ramp bottleneck 1"); this spillover lasts several hours. This case of spillover cannot be considered as induced traffic breakdown, because congested traffic at the on-ramp bottleneck is forced by spillover.

(iii) The jam propagation through a bottleneck leads neither to induced traffic breakdown nor to an EP (Fig. 1 (d)). This effect of spillover shows that the flow rate is smaller than the minimum capacity of free flow at the bottleneck: $q < C_{\rm min}$.

C. Conclusions

An empirical study of real field traffic data allows us to make the following conclusions about physical features of empirical nuclei for spontaneous traffic breakdown in free flow at highway bottlenecks:

1. In the most real field traffic data measured in 1996–2014 by road detectors on German freeways, a nucleus for traffic breakdown at a highway bottleneck occurs through an interaction of one of the waves in free flow with a permanent speed disturbance localized at a highway bottleneck. When the wave reaches the location of the disturbance at the bottleneck (effective bottleneck location), spontaneous traffic breakdown, i.e., phase transition from free flow to synchronized flow occurs.

2. Waves in free flow, which can be nuclei for spontaneous traffic breakdown at highway bottlenecks, appear due to oscillations in the percentage of slow vehicles over time. These waves propagate with the average speed of slow vehicles in free flow (about 85–88 km/h for German highways). Within a wave, the total flow rate is larger and the speed averaged across the highway is smaller than outside the wave.

3. Any of the waves in free flow, which can be a nucleus for spontaneous traffic breakdown at a highway bottleneck, exhibits a two-dimensional (2D) asymmetric spatiotemporal structure whose characteristics are different in different highway lanes.

4. Microscopic traffic simulations with a stochastic traffic flow model in the framework of three-phase theory explain the empirical findings.

Appendix A: Stochastic three-phase traffic flow model used for simulations

1. Update rules of vehicle motion

The traffic flow model used in Sec. III B (see Tables I and II) [44] is a discrete version [23] of the stochastic three-phase traffic flow model of Ref. [50, 51]: rather than the continuum space co-ordinate, a discretized space co-ordinate with a small enough value of the discretization cell δx is used. Consequently, the vehicle speed and acceleration (deceleration) discretization intervals are $\delta v = \delta x/\tau$ and $\delta a = \delta v/\tau$, respectively, where time step $\tau = 1$ s.

In formulae of Tables I and II, $n = 0, 1, 2, ...$ is number of time steps, x_n is the vehicle coordinate at time step n, v_n is the vehicle speed at time step n, $v_{\rm free}$ is a maximum speed in free flow, $g_n = x_{\ell,n} - x_n - d$ is a space gap, d is a vehicle length, index ℓ marks the preceding vehicle, $G(v_n, v_{\ell,n})$ is a synchronization gap, superscripts $+$ and $-$ in variables, parameters, and functions denote the preceding vehicle and the trailing vehicle in the "target" (neighboring) lane, respectively; the target lane is the lane into which the vehicle wants to change.

Because in the discrete model version discretized (and dimensionless) speed and acceleration are used, which are measured respectively in the discretization values δv and δa, the value τ in all formulae below is assumed to be the dimensionless value $\tau = 1$.

TABLE I: Discrete version of stochastic three-phase traffic flow model of Ref. [51]

Vehicle motion in road lane
$v_{n+1}=\max(0,\min(v_{\rm free},\tilde v_{n+1}+\xi_n,v_n+a\tau,v_{{\rm s},n}))$, $x_{n+1}=x_n+v_{n+1}\tau$, $\tilde v_{n+1}=\min(v_{\rm free},v_{{\rm s},n},v_{{\rm c},n})$, $v_{{\rm c},n}=\begin{cases} v_n+\Delta_n & \text{at } g_n\le G_n,\\ v_n+a_n\tau & \text{at } g_n>G_n,\end{cases}$ $\Delta_n=\max(-b_n\tau,\min(a_n\tau,\ v_{\ell,n}-v_n))$, $g_n=x_{\ell,n}-x_n-d$, $v_{\rm free}$, a, and d are constants, $\tau=1$;
Stochastic time delay of acceleration and deceleration: $a_n=a\Theta(P_0-r_1)$, $b_n=a\Theta(P_1-r_1)$, $P_0=\begin{cases} p_0 & \text{if } S_n\ne 1\\ 1 & \text{if } S_n=1,\end{cases}$ $P_1=\begin{cases} p_1 & \text{if } S_n\ne -1\\ p_2 & \text{if } S_n=-1,\end{cases}$ $S_{n+1}=\begin{cases} -1 & \text{if } \tilde v_{n+1}<v_n\\ 1 & \text{if } \tilde v_{n+1}>v_n\\ 0 & \text{if } \tilde v_{n+1}=v_n,\end{cases}$ $\Theta(z)=0$ at $z<0$ and $\Theta(z)=1$ at $z\ge 0$, $r_1=\text{rand}(0,1)$, $p_0=p_0(v_n)$, $p_2=p_2(v_n)$, p_1 is constant.
Model speed fluctuations: $\xi_n=\begin{cases}\xi_{\rm a} & \text{if } S_{n+1}=1\\ -\xi_{\rm b} & \text{if } S_{n+1}=-1\\ \xi^{(0)} & \text{if } S_{n+1}=0,\end{cases}$ $\xi_{\rm a}=a^{({\rm a})}\tau\Theta(p_{\rm a}-r)$, $\xi_{\rm b}=a^{({\rm b})}\tau\Theta(p_{\rm b}-r)$, $\xi^{(0)}=a^{(0)}\tau\begin{cases}-1 & \text{if } r\le p^{(0)}\\ 1 & \text{if } p^{(0)}<r\le 2p^{(0)} \text{ and } v_n>0\\ 0 & \text{otherwise,}\end{cases}$ $r=\text{rand}(0,1)$; $a^{({\rm a})}=a^{({\rm a})}(v_n)$, $a^{({\rm b})}=a^{({\rm b})}(v_n)$; $p_{\rm a}$, $p_{\rm b}$, $p^{(0)}$, $a^{(0)}$ are constants.
Synchronization gap G_n and safe speed $v_{{\rm s},n}$: $G_n=G(v_n,v_{\ell,n})$, $G(u,w)=\max(0,\lfloor k\tau u+a^{-1}\phi_0 u(u-w)\rfloor)$, $v_{{\rm s},n}=\min\left(v_n^{(\rm safe)},g_n/\tau+v_\ell^{({\rm a})}\right)$, $v_n^{(\rm safe)}=\lfloor v^{(\rm safe)}(g_n,\ v_{\ell,n})\rfloor$, $v^{(\rm safe)}\tau_{\rm safe}+X_{\rm d}(v^{(\rm safe)})=g_n+X_{\rm d}(v_{\ell,n})$, $X_{\rm d}(u)=b\tau^2\left(\alpha\beta+\frac{\alpha(\alpha-1)}{2}\right)$, $\alpha=\lfloor u/b\tau\rfloor$, $\beta=u/b\tau-\alpha$, $v_\ell^{({\rm a})}=\max(0,\min(v_{\ell,n}^{(\rm safe)},v_{\ell,n},g_{\ell,n}/\tau)-a\tau)$, $\tau_{\rm safe}$ is a safe time gap; b, $k>1$, and ϕ_0 are constants; $\lfloor z\rfloor$ denotes the integer part of a real number z.

TABLE II: Lane changing rules in discrete version of stochastic three-phase traffic flow model of Ref. [51]

Lane changing rules
Lane changing occurs with probability $p_{\rm c}$ from right to left lane $R\to L$ and back $L\to R$:
Incentive conditions for lane changing $R\to L$: $v_n^+\ge v_{\ell,n}+\delta_1$ and $v_n\ge v_{\ell,n}$, $L\to R$: $v_n^+>v_{\ell,n}+\delta_1$ or $v_n^+>v_n+\delta_1$. In conditions $R\to L$ and $L\to R$, the value v_n^+ at $g_n^+>L_{\rm a}$ and the value $v_{\ell,n}$ at $g_n>L_{\rm a}$ are replaced by ∞, where $L_{\rm a}$ is constant.
Safety conditions for lane changing rules $(*)$: $g_n^+>\min(v_n\tau,\ G_n^+)$, $g_n^->\min(v_n^-\tau,\ G_n^-)$, where $G_n^+=G(v_n,v_n^+)$, $G_n^-=G(v_n^-,v_n)$, *or* rule $(**)$: $x_n^+-x_n^--d>g_{\rm target}^{(\rm min)}$ with $g_{\rm target}^{(\rm min)}=\lfloor\lambda v_n^++d\rfloor$, the vehicle should pass the midpoint point $x_n^{({\rm m})}$ between two neighboring vehicles in the target lane.
Speed after lane changing $v_n=\hat v_n$, $\hat v_n=\min(v_n^+,\ v_n+\Delta v^{(1)})$, in $\hat v_n$ the speed v_n is related to the initial lane before lane changing. Vehicle coordinate after lane changing does not changes under rules $(*)$ and it changes to $x_n=x_n^{({\rm m})}$ under rule $(**)$.

2. Model of vehicle merging at moving bottleneck

In accordance with [44], we assume that a slow vehicle moves in the right lane. If a vehicle moves initially in the right lane upstream of the slow vehicle, then within the moving merging region $L_{\rm c}$ (Fig. 14 (b)) the vehicle changes from the right lane to the left lane, when safety conditions $(*)$ *or* $(**)$ are satisfied.

The safety conditions $(*)$ are as follows:

$$\begin{aligned} g_n^+&>\min(\hat v_n\tau,\ G(\hat v_n,v_n^+)),\\ g_n^-&>\min(v_n^-\tau,\ G(v_n^-,\hat v_n)),\end{aligned}\tag{A1}$$

$$\hat v_n=\min(v_n^+,\ v_n+\Delta v_r^{(1)}),\tag{A2}$$

$\Delta v_r^{(1)}>0$ is constant

The safety condition $(**)$ is given by formula

$$x_n^+-x_n^--d>g_{\rm target}^{(\rm min)},\quad g_{\rm target}^{(\rm min)}=\lfloor\lambda_{\rm b}v_n^++d\rfloor,\tag{A3}$$

$\lambda_{\rm b}$ is constant; in addition, the vehicle should pass the midpoint $x_n^{({\rm m})}=\lfloor(x_n^++x_n^-)/2\rfloor$ between two neighboring vehicles in the target lane, i.e., the conditions

$$\begin{aligned} &x_{n-1}<x_{n-1}^{({\rm m})} \text{ and } x_n\ge x_n^{({\rm m})}\\ &\textit{or}\\ &x_{n-1}\ge x_{n-1}^{({\rm m})} \text{ and } x_n<x_n^{({\rm m})}.\end{aligned}\tag{A4}$$

should be satisfied.

Speed adaptation before vehicle merging is given by vehicle motion rules of Tables I, where

$$v_{{\rm c},n}=\begin{cases} v_n+\Delta_n^+ \text{ at } g_n^+\le G(v_n,\hat v_n^+)\\ v_n+a_n\tau \text{ at } g_n^+>G(v_n,\hat v_n^+)\end{cases}\tag{A5}$$

$$\Delta_n^+=\max(-b_n\tau,\min(a_n\tau,\ \hat v_n^+-v_n)),\tag{A6}$$

$$\hat v_n^+=\max(0,\min(v_{\rm free},\ v_n^++\Delta v_r^{(2)})),\tag{A7}$$

$\Delta v_r^{(2)}$ is constant.

After vehicle merging the vehicle speed v_n is set to $\hat v_n$ (A2); note that in (A2) the vehicle speed v_n is the speed before vehicle merging; under the rule $(*)$ the vehicle coordinate x_n does not change, under the rule $(**)$:

$$x_n=x_n^{({\rm m})}.\tag{A8}$$

TABLE III: Model parameters used in most simulations (when other model parameters or the continuum stochastic model of [51] are used, this is mentioned in figure captions)

Vehicle motion in road lane:
$\tau_{\rm safe} = \tau$, $d = 7.5$ m/δx, $\delta x = 0.01$ m,
$v_{\rm free}^{(\max)} = 30$ ms$^{-1}/\delta v$, $b = 1$ ms$^{-2}/\delta a$,
$\delta v = 0.01$ ms^{-1}, $\delta a = 0.01$ ms^{-2}, $k = 3$,
$p_1 = 0.3$, $\phi_0 = 1$, $p_b = 0.1$, $p_a = 0.17$
$p^{(0)} = 0.005$, $p_2(v_n) = 0.48 + 0.32\Theta(v_n - v_{21})$,
$p_0(v_n) = 0.575 + 0.125 \min(1, v_n/v_{01})$,
$a^{(\rm b)}(v_n) = 0.2a +$
$+0.8a \max(0, \min(1, (v_{22} - v_n)/\Delta v_{22})$,
$a^{(0)} = 0.2a$, $a^{(\rm a)} = a$,
$v_{22} = 12.5$ ms$^{-1}/\delta v$, $\Delta v_{22} = 2.778$ ms$^{-1}/\delta v$,
$v_{01} = 10$ ms$^{-1}/\delta v$, $v_{21} = 15$ ms$^{-1}/\delta v$, $a = 0.5$ ms$^{-2}/\delta a$.
Lane changing:
$\delta_1 = 1$ ms$^{-1}/\delta v$, $L_{\rm a} = 80$ m/δx,
$p_{\rm c} = 0.2$, $\lambda = 0.75$, $\Delta v^{(1)} = 2$ ms$^{-1}/\delta v$.
Bottleneck models:
$\lambda_{\rm b} = 0.75$ for all the bottlenecks,
$L_{\rm c} = 0.3$ km/δx for moving bottleneck,
$v_{\rm free\ on} = 22.2$ ms$^{-1}/\delta v$,
$\Delta v_{\rm r}^{(2)} = 5$ ms$^{-1}/\delta v$ for on-ramp bottleneck,
$L_{\rm r} = 1$ km/δx, $\Delta v_{\rm r}^{(1)} = 10$ ms$^{-1}/\delta v$,
$L_{\rm m} = 0.3$ km/δx for on-ramp bottleneck.

The same rules for vehicle merging are used in models of an on-ramp bottleneck (Fig. 14 (b)) (see Fig. 16.2 in Sect. 16.3.6 of [14]), i.e., when a vehicle merges from the on-ramp onto the main road or a vehicle leaves the main road to the off-ramp.

Appendix B: Model of moving virtual detector

To reconstruct a 2D-structure of the flow rate (Fig. 14 (d)), we use a moving virtual detector at which the vehicle speed $v = v(x,\ t)$ and headway between vehicles $h = h(x,\ t)$ are averaged in a neighborhood of the moving bottleneck as follows:

$$v_{\rm avr}(x,\ t) = \frac{1}{T}\int_{t-T/2}^{t+T/2} v(x + v_{\rm det}(t'-t),\ t')dt', \quad \text{(B1)}$$

$$h_{\rm avr}(x,\ t) = \frac{1}{T}\int_{t-T/2}^{t+T/2} h(x + v_{\rm det}(t'-t),\ t')dt', \quad \text{(B2)}$$

where $T = 5$ min is the averaging time interval, $v_{\rm det}$ is the speed of virtual detector (we use $v_{\rm det} = v_{\rm M}$). The flow rate is

$$q_{\rm avr}(x,\ t) = v_{\rm avr}(x,\ t)/h_{\rm avr}(x,\ t). \quad \text{(B3)}$$

In the discrete form, coordinate x and time t are discrete ones: $x_m = mh_{\rm x}$ and $t_k = kh_{\rm t}$, $m = 0, 1, 2, ...$, $k = 0, 1, 2, ...$, where the space step $h_{\rm x}$ =7.5 m and the time step $h_{\rm t}$ =1 s. Then formulae (B1), (B2) take the form

$$v_{\rm avr}(x_m,\ t_k) = \frac{1}{N_T+1}\sum_{k'=-N_{\rm T}/2}^{k'=N_{\rm T}/2} v(x_m + h_{\rm x}m',\ t_k + h_{\rm t}k'), \quad \text{(B4)}$$

$$h_{\rm avr}(x_m,\ t_k) = \frac{1}{N_T+1}\sum_{k'=-N_{\rm T}/2}^{k'=N_{\rm T}/2} h(x_m + h_{\rm x}m',\ t_k + h_{\rm t}k'), \quad \text{(B5)}$$

where

$$m' = \lfloor v_{\rm det}h_{\rm t}k'/h_{\rm x}\rfloor, \quad \text{(B6)}$$

the expression $\lfloor z\rfloor$ denotes the integer part of z, the value $N_{\rm T}$ is chosen to be the even value and $T = (N_{\rm T}+1)h_{\rm t}$.

[1] G.M. Pound, V.K. La Mer. J. American Chemical Society **74** 2323 (1952).
[2] E. Sanz, C. Vega, J.R. Espinosa, R. Cabellero-Bernal, J.L.F. Abascal, C. Valeriani, J. American Chemical Society **135** 15008–15017 (2013).
[3] H. Haken, *Synergetics* (Springer, Berlin 1977)
[4] R. Thom, *Structural Stability and Morphogenesis* (Benjamin, Reading, MA 1975)
[5] C.W. Gardiner, *Handbook of Stochastic Methods*, Second Edition (Springer, Berlin 1990).
[6] G. Nicolic, I. Prigogine, *Self-Organization in Nonequilibrium Systems* (Wiley, N.Y. 1977)
[7] E. Schöll, *Nonequilibrium Phase Transitions in Semiconductors* (D. Reidel, Dordrecht 1987)
[8] V.A. Vasil'ev, Yu.M. Romanovskii, D.S. Chernavskii, V.G. Yakhno, *Autowave Processes in Kinetic Systems* (Springer, Berlin 1990)
[9] A.S. Mikhailov, *Foundations of Synergetics Vol. I* (Springer, Berlin 1994), 2nd ed.
[10] A.S. Mikhailov, A.Yu. Loskutov: *Foundation of Synergetics II. Complex patterns* (Springer, Berlin 1991)
[11] B.S. Kerner, V.V. Osipov: *Autosolitons: A New Approach to Problems of Self-Organization and Turbulence* (Kluwer, Dordrecht, Boston, London 1994); Sov. Phys. Usp. **32**, 101–138 (1989); Sov. Phys. Usp. **33**, 679–719 (1990)
[12] S. Chandrasekhar, *Hydrodynamic and Hydromagnetic Stability* (Oxford University Press, Oxford 1961)

[13] F.-J. Niedernostheide (ed.) *Nonlinear Dynamics and Pattern Formation in Semiconductors and Devices* (Springer, Berlin 1995).

[14] B.S. Kerner, *The Physics of Traffic* (Springer, Berlin, New York 2004)

[15] B.S. Kerner, *Introduction to Modern Traffic Flow Theory and Control.* (Springer, Berlin, New York, 2009).

[16] B.S. Kerner, Physica A **392**, 5261 (2013).

[17] B.S. Kerner, H. Rehborn, R.-P. Schäfer, S. L. Klenov, J. Palmer, S. Lorkowski, N. Witte, Physica A **392** 221–251 (2013).

[18] The effective bottleneck location is a road location at which traffic breakdown is observed ($x \approx 6.4$ km). In the reality, the on-ramp bottleneck shown in Fig. 1 (a) consists of two different on-ramps that are in intersection "Friedberg" of freeway A5-South with other road(s). Explanations of this effective on-ramp bottleneck can be found in Sec. 2.3.2 and 9.2.1 of the book [14]. The inflow to the upstream on-ramp explains the increase in the flow rates q and $q_{\rm slow}$ occurring about 0.5–1 km upstream of the effective bottleneck location.

[19] B.S. Kerner, Transp. Res. Rec. **1710** 136 (2000).

[20] B.S. Kerner, S.L. Klenov, Physica A **364**, 473–492 (2006).

[21] B.S. Kerner, S.L. Klenov, Transp. Res. Rec. **1965**, 70–78 (2006).

[22] B.S. Kerner, S.L. Klenov, in *Encyclopedia of Complexity and System Science*, ed. by R.A. Meyers. (Springer, Berlin, 2009), pp. 9282–9302.

[23] B.S. Kerner, S.L. Klenov, **80** 056101 (2009).

[24] B.N. Persaud, S. Yagar, R. Brownlee, Trans. Res. Rec. 1634 (1998) 64–69.

[25] B.S. Kerner, S.L. Klenov, D.E. Wolf, J. Phys. A: Math. Gen. 35 (2002) 9971–10013.

[26] W. Brilon, M. Regler, J. Geistefeld, Straßenverkehrstechnik, Heft 3 (2005) 136.

[27] W. Brilon, H. Zurlinden, Straßenverkehrstechnik, Heft 4 (2004) 164.

[28] W. Brilon, J. Geistefeldt, M. Regler, in: H.S. Mahmassani (Ed.), Traffic and Transportation Theory, Elsevier Science, Amsterdam, 2005. pp. 125–144.

[29] J. Geistefeldt, W. Brilon, in: W.H.K. Lam, S.C. Wong, H.K. Lo (Eds.), Transportation and Traffic Theory 2009, Springer, Dordrecht, Heidelberg, London, New York 2009. pp. 583–602.

[30] L. Elefteriadou, An Introduction to Traffic Flow Theory. Springer Optimization and Its Applications, Vol. 84, (Springer, Berlin 2014).

[31] It can be assumed that a permanent local speed disturbance in free flow at the effective location of an on-ramp bottleneck is associated with vehicles merging from on-ramp lane to the main road [14, 15]. These vehicles force the vehicles on the main road to decrease their speed in a neighborhood of the on-ramp merging region. This assumption is confirmed by simulations made in Sec. III B 3 (see Fig. 16). It can also be assumed that a permanent local speed disturbance in free flow at the effective location of an off-ramp bottleneck is associated with vehicles that must change the lane to leave the main road to the off-ramp. This lane changing, which occurs mostly in a small road region downstream of the off-ramp lane, causes the speed decrease of vehicles on the main road. However, to prove these theoretical assumptions with empirical data, measurements of microscopic (single-vehicle) spatiotemporal data (e.g., vehicle trajectories) of almost all vehicles moving in free flow in a neighborhood of a highway bottleneck are required. Unfortunately, such data is not currently available.

[32] This empirical result confirms the conclusion of [15, 23] that the statement about an empirical observation of a "boomerang effect" [33], i.e., growing disturbances on a homogeneous freeway section without on- and off-ramps is invalid. Note that the boomerang effect in traffic flow was predicted in simulations of a traffic flow model belonging to General Motors model class [34]: A disturbance (a wave) in free flow propagates firstly downstream, then it comes to a stop, while strongly growing, and finally the disturbance begins to propagate upstream, while transforming into a moving jam.

[33] M. Schonhof and D. Helbing, Transp. Sc. **41**, 135 (2007); Transp. Res., Part B: Methodol. **43**, 784 (2009).

[34] B. S. Kerner and P. Konhäuser, Phys. Rev. E **50**, 54 (1994); B. S. Kerner, P. Konhäuser, and M. Schilke, Phys. Rev. E **51**, 6243 (1995).

[35] D.C. Gazis, R. Herman Trans. Sci. **26** 223 (1992).

[36] G.F. Newell, A moving bottleneck. Inst. of Transp. Studies Research Report UCB ITS-RR-93-3) (Berkley, CA: University of California 1993).

[37] G.F. Newell, Transp. Res. B **32** 531 (1988).

[38] J.C. Muñoz, C.F. Daganzo, in: Traffic and Transportation Theory, ed. by M.A.P. Taylor (Pergamon, Oxford, 2002) pp 441–462.

[39] J.P. Lebacque, J.B. Lesort, F. Giorgi, Transp. Res. Rec. **1644**, 70–79 (1998).

[40] L. Leclercq, S. Chanut, J.B. Lesort, Transp. Res. Rec. **1883**, 3–13 (2004).

[41] C.F. Daganzo, J.A. Laval. On the Numerical Treatment of Moving Bottlenecks. Report UCB-ITS-RR-93-7. Institute of Transportation Studies, University of California, Berkeley, 2003.

[42] K. Fadhloun, H. Rakha, A. Loulizi, Transp. Lett. **6**, 185–196 (2014).

[43] K. Fadhloun, H. Rakha, A. Loulizi, Transp. Res. Rec. **2422**, 61–70 (2014).

[44] B.S. Kerner, S.L. Klenov, J. Phys. A: Math. Theor. **43** 425101 (2010).

[45] B. S. Kerner, in *Proceedings of the 3rd Symposium on Highway Capacity and Level of Service*, edited by R. Rysgaard (Road Directorate, Ministry of Transport, Denmark, 1998), Vol. 2, pp. 621–642; B. S. Kerner, Phys. Rev. Lett. **81**, 3797 (1998); B. S. Kerner, in *Traffic and Granular Flow' 97*, edited by M. Schreckenberg and D. E. Wolf (Springer, Singapore, 1998), pp. 239–267.

[46] B. S. Kerner, Transp. Res. Rec. **1678**, 160 (1999); B. S. Kerner, in *Transportation and Traffic Theory*, edited by A. Ceder (Elsevier Science, Amsterdam, 1999), pp. 147–171; Physics World **12**, 25–30 (August 1999).

[47] It should be noted that for 2D steady states of synchronized flow (Fig. 14 (a)) we have often used the term "the fundamental hypothesis of three-phase traffic theory" [14, 15]. The term should emphasize the qualitative difference between the fundamental hypothesis of earlier traffic flow theories about a theoretical fundamental diagram of traffic flow, i.e., 1D-curve(s) in the flow–density plane. Indeed, in 1955 Lighthill and Whitham [48] wrote in the classical work (p. 319 in [48]): "... The fundamental hypothesis of the theory is that at any point of

the road the flow (vehicles per hour) is a function of the concentration (vehicles per mile)...". Thus the term "fundamental hypothesis of three-phase traffic theory" has a sense *only*, if a comparison between 2D steady states of synchronized flow of three-phase theory with 1D steady states of traffic flow of ealier traffic flow theories is made. Unfortunately, some authors "extend" the use of this term behind this comparison, for example, while equalizing three-phase theory and its fundamental hypothesis. This confusion leads to invalid conclusions. For these reasons, instead of the term "the fundamental hypothesis of three-phase traffic theory" we use the term "hypothesis of three-phase theory about states of synchronized flow". As emphasized in [16], the main reason for the three-phase theory is the explanation of the set of fundamental empirical features of traffic breakdown at highway bottlenecks, rather than states of synchronized flow resulting from the breakdown. In other words, the basic feature of the three-phase theory is the explanation of traffic breakdown at highway bottlenecks by an F→S transition in a metastable state of free flow [14, 15] that is also the basic reason for the incommensurability of three-phase theory with all two-phase traffic flow theories [49].

[48] M.J. Lighthill, G.B. Whitham, Proc. Roy. Soc. A **229**, 281–345 (1955).

[49] B.S. Kerner, S.L. Klenov, M. Schreckenberg, Phys. Rev. E **89**, 052807 (2014).

[50] B.S. Kerner, S.L. Klenov, J. Phys. A: Math. Gen. **35**, L31–L43 (2002).

[51] B.S. Kerner, S.L. Klenov, Phys. Rev. E **68** 036130 (2003).

[52] B.S. Kerner. in Encyclopedia of Complexity and System Science, ed. by R.A. Meyers. (Springer, Berlin, 2009), pp. 9302–9355; 9355–9411.

[53] Over time there has been developed a number of other three-phase traffic flow models (e.g., [17, 54**?** –105]) that incorporate some of the hypotheses of the three-phase theory [14, 15].

[54] B.S. Kerner, Phys. Rev. E **85** 036110 (2012).

[55] B.S. Kerner, S.L. Klenov, G. Hermanns, M. Schreckenberg, Physica A, **392** 4083–4105 (2013).

[56] L.C. Davis, Phys. Rev. E **69** 016108 (2004).

[57] H.K. Lee, R. Barlović, M. Schreckenberg, D. Kim, Phys. Rev. Lett. **92** 238702 (2004).

[58] R. Jiang, Q.-S. Wu, J. Phys. A: Math. Gen. **37** 8197–8213 (2004).

[59] K. Gao, R. Jiang, S.-X. Hu, B.-H. Wang, Q.-S. Wu, Phys. Rev. E **76** 026105 (2007).

[60] L.C. Davis, Physica A **368** 541–550 (2006).

[61] L.C. Davis, Physica A **361** 606–618 (2006).

[62] L.C. Davis, Physica A **387** 6395–6410 (2008).

[63] L.C. Davis, Physica A **388** 4459–4474 (2009).

[64] L.C. Davis, Physica A **389** 3588–3599 (2010).

[65] L.C. Davis, Physica A **391** 1679 (2012).

[66] R. Jiang, M.-B. Hua, R. Wang, Q.-S. Wu, Phys. Lett. A **365** 6–9 (2007).

[67] R. Jiang, Q.-S. Wu, Phys. Rev. E **72** 067103 (2005).

[68] R. Jiang, Q.-S. Wu, Physica A **377** 633–640 (2007).

[69] R. Wang, R. Jiang, Q.-S. Wu, M. Liu, Physica A **378** 475–484 (2007).

[70] A. Pottmeier, C. Thiemann, A. Schadschneider, M. Schreckenberg, in: A. Schadschneider, T. Pöschel, R. Kühne, M. Schreckenberg, D.E. Wolf (Eds.), Traffic and Granular Flow'05, Springer, Berlin, 2007, pp. 503–508.

[71] X.G. Li, Z.Y. Gao, K.P. Li, X.M. Zhao, Phys. Rev. E **76** 016110 (2007).

[72] J.J. Wu, H.J. Sun, Z.Y. Gao, Phys. Rev. E **78** 036103 (2008).

[73] J.A. Laval, in: A. Schadschneider, T. Pöschel, R. Kühne, M. Schreckenberg, D.E. Wolf (Eds.), Traffic and Granular Flow'05, Springer, Berlin, 2007, pp. 521–526.

[74] S. Hoogendoorn, H. van Lint, V.L. Knoop, Trans. Res. Rec. **2088** 102–108 (2008).

[75] B.S. Kerner, J. Phys. A: Math. Theor. **41** 215101 (2008).

[76] K. Gao, R. Jiang, B.-H. Wang, Q.-S. Wu, Physica A **388** 3233–3243 (2009).

[77] B. Jia, X.-G. Li, T. Chen, R. Jiang, Z.-Y. Gao, Transportmetrica **7** 127 (2011).

[78] J.-F. Tian, B. Jia, X.-G. Li, R. Jiang, X.-M. Zhao, Z.-Y. Gao, Physica A **388** 4827–4837 (2009).

[79] S. He, W. Guan, L. Song, Physica A **389** 825–836 (2009).

[80] C.-J. Jin, W. Wang, R. Jiang, K. Gao, J. Stat. Mech. P03018 (2010).

[81] S.L. Klenov, in: V.V. Kozlov (Ed.), Proc. of Moscow Inst. of Phys. and Technology (State University), Vol. 2, N. 4 pp. 75–90 (2010) (in Russian).

[82] A.V. Gasnikov, S.L. Klenov, E.A. Nurminski, Y.A. Kholodov, N.B. Shamray, Introduction to mathematical simulations of traffic flow, Moscow, MCNMO, 2013 (in Russian).

[83] S. Kokubo, J. Tanimoto, A. Hagishima, Physica A **390** 561–568 (2011).

[84] H.-K. Lee, B.-J. Kim, Physica A **390** 4555–4561 (2011).

[85] C.-J. Jin, W. Wang, Physica A **390** 4184–4191 (2011).

[86] J.P.L. Neto, M.L. Lyra, C.R. da Silva, Physica A **390** 3558–3565 (2011).

[87] P. Zhang, C.-X. Wu, S.C. Wong, Physica A **391** 456–463 (2012).

[88] W.-H. Lee, S.-S. Tseng, J.-L. Shieh, H.-H. Chen, IEEE Trans. on ITS **12** 1047–1056 (2011).

[89] S. Lee, B. Heydecker, Y.H. Kim, E.-Y. Shon, J. of Adv. Trans. **4** 143–158 (2011).

[90] J.-F. Tian, Z.-Z. Yuana, M. Treiber, B. Jia, W.-Y. Zhanga, Physica A **391** 3129 (2012).

[91] M. Kimathi, Mathematical models for 3-phase traffic flow theory, Doctor Thesis, 2012. https://kluedo.ub.uni-kl.de/frontdoor/index/index/docId/2899.

[92] R. Borsche, M. Kimathi, A. Klar, Comp. and Math. with Appl. **64** 2939–2953 (2012).

[93] Y. Wang, Y.I. Zhang, J. Hu, L. Li, Int. J. of Mod. Phys. C **23** 1250060 (2012).

[94] J.-f. Tian, Z.-z. Yuan, B. Jia, H.-q. Fan, T. Wang, Phys. Lett. A **376** 2781–2787 (2012).

[95] Y. Qiu, J. of Non-Newtonian Fluid Mechanics **197** 1–4 (2013).

[96] B.S. Kerner, S.L. Klenov, M. Schreckenberg, Phys. Rev. E **84** 046110 (2011).

[97] H. Yang, J. Lu, X. Hu, J. Jiang, Physica A, **392**, 4009 (2013).

[98] F. Knorr, M. Schreckenberg, J. Stat. Mech. (2013) P07002.

[99] Xiang Zheng-Tao, Li Yu-Jin, Chen Yu-Feng, Xiong Li, Physica A, **392**, 5399 (2013).

[100] A.R. Mendez, R.M. Velasco, J. Phys. A: Math. Theor. **46** 462001 (2013).

[101] R. Jiang, M.-B. Hu, H.M. Zhang, Z.-Y. Gao, B. Jia, Q.-

S. Wu, B. Wang, M. Yang, PLOS One **9** e94351 (2014).
[102] B.S. Kerner, S.L. Klenov, J. Phys. A: Math. Gen. **39** 1775–1809 (2006).
[103] B.S. Kerner, Europhys. Lett. **102** 28010 (2013).
[104] B.S. Kerner, S.L. Klenov, G. Hermanns, P. Hemmerle, H. Rehborn, and M. Schreckenberg, Phys. Rev. E **88**, 054801 (2013).
[105] J. Tian, M. Treiber, S. Ma, B. Jia, W. Zhang, Transp. Res. B **71** 138 (2015).
[106] K. Hausken, H. Rehborn, in: *Game Theoretic Analysis of Congestion, Safety and Security*, Springer Series in Reliability Engineering, (Springer, Berlin 2015), pp. 113–141.
[107] We can assume that some of slow (long) vehicles within the wave in the right lane change to the middle lane while trying to pass the wave occurring in the right lane. This can explain why some weak waves of slow vehicles occur in the middle lane (left column in Fig. 13 (b)). Due to a speed limit for long vehicles on German highways (formally, this speed limit is equal to 80 km/h, however, in the practice real maximum speeds of long vehicles change usually between 85 and 90 km/h) the difference in the speeds of slow vehicles is small; therefore, it takes usually several minutes for this passing. This can explain the spatiotemporal correlation of the waves of slow vehicles in the middle and right lanes (left column in Figs. 13 (a, b)).
[108] B.S. Kerner, Phys. Rev. E **65**, 046138 (2002).